Perspective

Dynamics of photoexcited exciton-phonon systems: Time-dependent theoretical approaches

Darius Abramavicius,[1] Arunjyoti Baidya,[1] Vytautas Bubilaitis,[1] and Leonas Valkunas[1,2]
[1]*Institute of Chemical Physics, Physics Faculty, Vilnius University, Saulėtekio Avenue 3, 10257 Vilnius, Lithuania*
[2]*Department of Molecular Compound Physics, Center for Physical Sciences and Technology, Saulėtekio Avenue 3, 10257 Vilnius, Lithuania*

(Received 1 November 2025; revised 20 April 2026; published 6 July 2026)

Electronic excitations of molecular aggregates experience fluctuations of thermal phonons, which cause decoherence and trapping. Such process is denoted by exciton-polaron formation. Depending on the exciton-phonon coupling strength and the temperature, it may be convenient to describe properties of electronic excited states using either excitonic or polaronic representation. Two types of theoretical approaches are described: the first based on Heisenberg representation elegantly describes the excitation process, while the second, based on the time-dependent variational principle, describes the excitation evolution and trapping using polaron picture.

DOI: 10.1103/h7v9-2z61

I. INTRODUCTION

Exciton is the basic concept used to describe the spectroscopic properties of crystals, molecular complexes, and aggregates [1–3]. Excitons represent the collective electronic excited states of the extended system, which manifest themselves as unique transition bands in various spectroscopic experiments. They play a significant role in coloring plants and are major players in their life cycle [4–7]. Under aggregated conditions, molecules with similar optical properties interact with each other through electrostatic resonant couplings. These are the Coulomb interaction energies between transition charge densities of the molecules. Due to these couplings, spectroscopically molecular aggregates behave as supermolecules, whose excitations are denoted by excitons. Several types of excitons are defined considering the electron-hole binding energy, the thermal energy, and the resonant couplings. In the case of molecular aggregates and molecular crystals, the electron-hole separation is restricted to the same molecule and the electrons and holes are always bound to the single molecule. Such excitation is denoted as the Frenkel-type exciton.

Bandwidths of the excitonic transitions in molecular aggregates are controlled by electronic interaction with molecular vibrations and phonons of the lattice. Technically, both degrees of freedom are described by the same mathematical formalism, so in the following we do not differentiate between them and denote by phonons. As a result of these interactions, spectral bands become both broadened and shifted, as compared to the pure excitonic transitions [8]. In the case of strong exciton-phonon interaction, the exciton transitions become modified as a result of the exciton self-trapping as originally formulated by Rashba and Sturge [9]. The resulting characteristics resemble those of polarons.

Polarons were originally introduced by Landau when describing electron motion in crystal lattices [10]. For large local deformation (due to polarization, etc.), localized electron levels can be formed, which can trap electrons. A similar type of trapping can be anticipated for neutral exciton, which carries a specific dipole moment. This dipole moment may be sufficient to polarize the molecular medium, governed by weak Van Der Waals interactions and thus exciton-polaron can be formed. Throughout this paper, exciton-polarons and polarons are used interchangeably with the meaning of excitonic-polarons and exciton self-trapping.

Exciton self-trapping can be described by means of polaron-type transformation, which has been developed for characterization of the relevant energy states both for excitons and charged particles [11]. Polaron transformation represents the dressed excitons as a result of exciton-phonon interaction. Indeed, the resonant couplings promote coherent wavelike exciton propagation between molecules, while the phonons cause modulation of energy levels of different molecules leading to dissipation of the energy and phase relaxation between different excited states. As a result, the excitons lose phase coherence and get localized, which amplifies the local lattice deformation. Trapped excitons are thus polarons, which then carry the deformation or polarization as they diffuse. Overall, the excitation diffusion coefficient becomes smaller [2].

However, the timescale of such transition into the polaronic states is not represented in the mathematics of polaron transformation. The large complexity of temporal evolution is due to the broad spectral content of phonons. To overcome the complexity of this problem, various approximate approaches have been extensively developed.

One of the most widely used approximate approaches is based on time-dependent evolution of the reduced density matrix [12,13]. The approach generates various forms of the quantum master equation (QME). Two time-convolutional forms include transient basis transformation [14,15]. At the second order to the exciton-phonon interaction in the

Published by the American Physical Society under the terms of the Creative Commons Attribution 4.0 International license. Further distribution of this work must maintain attribution to the author(s) and the published article's title, journal citation, and DOI.

Markovian approximation, the QME turns into the well-known Redfield equation, which accounts for excitation energy relaxation and decoherence. It has been extended to cover the Foerster regime using the so-called modified Redfield scheme [16–20] in specific parameter regime. The approach can be extended to higher orders (e.g., to the fourth order [21]) and has been also written in partial polaron picture [22], where a single parameter is used to continuously switch from an excitonic to polaronic picture. This allows us to describe transient dynamics in terms of polarons, which better account for phonon thermalization.

A functional-integral (a path-integral) approach has been extensively used for reduced description of the dynamics. A two-state system coupled to a bosonic or fermionic environment has been extensively analyzed using this approach [23,24]. Such systems are denoted as spin-boson problems. Quantitative expressions are obtained for the system energy and phase relaxation as a function of the spectral density of its coupling to the environment. Exploitation of the path-integral approach for the Drude spectral density allows obtaining a hierarchy of equations using auxiliary density matrices, which is denoted as the hierarchy of equations of motion for the reduced density matrix (HEOM) [25–28]. HEOM equations have been successfully used for description of the photosynthetic exciton dynamics and calculation of absorption spectra [5,29–34].

Markovian description of exciton evolution on the femtosecond timescale leads to inaccurate spectral line shapes in spectroscopic measurements. On the other hand, HEOM approach (being accurate) hinders the physics of microscopic state evolution of the system. Variational approaches have been extensively used together with coherent state representation to successfully describe vibronic phenomena in absorption and nonlinear spectroscopies demonstrating full fluctuating state evolution [35–37]. Explicit equations of motion for coupled exciton and phonon amplitudes, obtained using time-dependent variational approach (TDVP), allow for feedback relations between the electronic and the vibrational manifolds. The approach turns out to be very efficient for describing bath relaxation and formation of polarons as described for several cases of the parameters [38,39]. Ensemble averaging is necessary for describing temperature-dependent effects. In the simplest case, the temperature is included and defined via initial displacements of the bath oscillators. The thermofield dynamics approach is used to construct the dynamics using the minimal set of variables [40]. However, the thermofield-TDVP perfectly defines the temperature for the electronic ground state, where bath oscillators are totally independent. The approaches introduce unwanted bath heating in electronically excited states after optical excitation due to energy conservation of the variational model [41]. Coupling to additional secondary baths has been introduced to alleviate the heating problem [42]. The method becomes very powerful in describing the bath heating and cooling during the exciton relaxation [43].

Another explicit-variable approach employs MultiConfigurational Time-Dependent Hartree (MCTDH) method to describe the model dynamics [44,45]. The method relies on the finite number of phonons which are included in the model. The model is still approximate due to the restricted basis. However, the TDVP and MCTDH, in principle, can be made to exactly represent the model dynamics if the space of variables is completely covered (making multipletic TDVP [46,47] or including a large number of vibrational quanta in MCTDH) and can be compared to another exact approach of HEOMs [25].

The site-basis model, where the problem is originally formulated, is the most effective when the resonant coupling between the sites is weak and the thermalized excited state is shifted from ground state equilibrium. Such a shifted equilibrium is embedded into the polaron transformation. In this paper, we develop the mixed exciton-polaron dynamics equations using the time-dependent variational approach. In this way, we can control the basis representation continuously for the TDVP wave function. Additionally, we describe the model with respect to another: the Heisenberg representation approach with specifically truncated basis model. Using a direct operator equation in the Heisenberg representation, the coupled exciton-phonon system is characterized. Similar to MCTDH, the number of phonons becomes controllable. These approaches allow tuning of the relaxation character for tracking the exciton thermalization and exciton-polaron transition. The paper essentially compares the two approaches for exciton dynamics and spectroscopy. The Heisenberg approach is formulated in the molecular basis (what is considered as the original basis), while the variational method is described in polaron-transformed basis, which continuously shifts from exciton to polaron states and is thus more universal.

The paper is organized as follows. Section II formulates the fluctuating exciton model and introduces exciton states. The resulting Hamiltonian is utilized in Sec. III, where the general equation is obtained as well as mean-field and one-quantum approximations being developed. These sets of equations are very efficient, describing excitation processes, and are utilized for absorption spectra calculations. Section IV transforms the problem into polaron representation, thus paving the way for an efficient excited state description in the manifold of excited states using the time-dependent variational principle. Sample calculations are presented in Sec. V, while conclusions are in Sec. VI.

II. FLUCTUATING HAMILTONIAN OF A GENERAL EXCITON-PHONON SYSTEM

We start with a molecular aggregate consisting of N molecules with similar optical properties, i.e., their absorption is in the same spectral window. In the Frenkel exciton formulation, the molecules can be either in the ground state or an electronic excited state. Using Heitler-London approximation, the basis quantum states of the aggregate can be written as products of molecular excitations: the ground state $|g\rangle = \Pi_n |g_n\rangle$, where n labels all the molecules in the aggregate, $|g_n\rangle$ is the ground state of molecule n. Excited states are given by products where one of the molecules are switched into the excited state:

$$|n\rangle = |g_1 g_2 ... g_{n-1} e_n g_{n+1} ... g_N\rangle. \tag{1}$$

Here $|e_i\rangle$ - local excited states of molecules. In this paper, we restrict ourselves to one-exciton states, where excitation of more than one molecule is not considered. Additionally, each

molecule is assumed to be a two-state system. States $|n\rangle$ with $n = 1...N$ form a convenient basis for an arbitrary one-exciton states of the molecular aggregate. Using this basis set, we can define the electronic (or observable system) Hamiltonian

$$\hat{H}_S = \sum_{mn} J^{(0)}_{mn} |m\rangle\langle n|. \tag{2}$$

Here, matrix $J^{(0)}_{mn}$ contains the resonant intermolecular couplings (for $m \neq n$) and molecular excitation energies (for $m = n$). This form includes only excited states. In principle, the electronic ground state can be formally included by requesting that it is isolated and its energy is set to zero. Additionally, note that we did not include off-resonant couplings and our $J^{(0)}_{nn}$ is not the vacuum excitation energy of the molecule—it does include the excitation energy shifts due to molecular aggregation [48].

The molecules in the aggregate have internal vibrational harmonic modes. In the dimensionless form the vibrational Hamiltonian of the ith vibration has the form of a harmonic oscillator:

$$\hat{H}_{\text{vibr}} = \frac{\omega_i}{2}\left(\hat{p}_i^2 + \hat{x}_i^2\right), \tag{3}$$

where $\hat{p}_i$ and $\hat{x}_i$ are momentum and coordinate operators of the oscillator, ω_i- the vibrational frequency. Throughout this paper, we set $\hbar = 1$. The equilibrium of a vibration potential is shifted in the electronic excited state: $\frac{\omega_i}{2}\hat{x}_i^2 \to \frac{\omega_i}{2}(\hat{x}_i - d_i)^2$. The excited state vibrational Hamiltonian becomes

$$\hat{H}^{(e)}_{\text{vibr}} = \frac{\omega_i}{2}\left(\hat{p}_i^2 + \hat{x}_i^2\right) + \frac{\omega_i}{2}d_i^2 - \omega_i d_i \hat{x}_i. \tag{4}$$

Denoting the reorganization energy of the nth molecule by $\Lambda_n = \sum_i \omega_i d_{ni}^2/2$, the whole Hamiltonian can then be written as

$$\begin{aligned}\hat{H} = &\sum_{mn}\left(J^{(0)}_{mn} + \delta_{mn}\Lambda_n\right)|m\rangle\langle n| \\ &+ \sum_i \frac{\omega_i}{2}\left(\hat{p}_i^2 + \hat{x}_i^2\right) - \sum_{ni}\omega_i d_{ni}|n\rangle\langle n|\hat{x}_i.\end{aligned} \tag{5}$$

Considering a wide range of vibrational frequencies of the whole system and its environment, there is a wide range of low-frequency vibrational modes associated with the intermolecular vibrations, which are denoted as phonons. Technically, both types of vibrations have the same description so in the following any type of vibrational excitations will be denoted by phonons. Using the phonon creation/annihilation operators, $\hat{x}_i = (\hat{a}_i^\dagger + \hat{a}_i)/\sqrt{2}$, $\hat{p}_i = i(\hat{a}_i^\dagger - \hat{a}_i)/\sqrt{2}$, and updating the diagonal terms by the reorganization energies, $J^{(0)}_{nn} + \Lambda_n \to J_{nn}$, we finally have the exciton-phonon Hamiltonian in the most convenient form:

$$\begin{aligned}\hat{H} = &\sum_{mn} J_{mn}|m\rangle\langle n| + \sum_i \omega_i(\hat{a}_i^\dagger\hat{a}_i + 1/2) \\ &- \sum_{ni} c_{ni}|n\rangle\langle n|(\hat{a}_i^\dagger + \hat{a}_i).\end{aligned} \tag{6}$$

Here the first term describes the electronic excitations (we denote it by the system $\hat{H}_S$); the second term is the phonon Hamiltonian and is denoted by a bath $\hat{H}_B$, while the third term is the exciton-phonon coupling $\hat{H}_{\text{SB}}$ with the coupling constants $c_{ni} = \omega_i d_{ni}/\sqrt{2}$. The corresponding full reorganization energy of nth excitation is $\Lambda_n = \sum_i c_{ni}^2/\omega_i$. All parameters, J_{mn}, ω_i, c_{ni} have energy dimension and can be directly compared.

Often the dimensionless Huang-Rhys (HR) parameter is also used to describe the system-bath coupling, $S_{ni} = d_{ni}^2/2$. In the present form $S_{ni} = c_{ni}^2/\omega_i^2$. The HR parameter describes the absorption intensity of phonon-induced side-band in absorption line shape [49,50].

It should be noted that for a bath linearly coupled to the system in the local bath approximation, only autocorrelation functions of fluctuations are important. This model is at the core for the second order system-bath relaxation theory for excitonic aggregates [13]. The autocorrelation functions involve only $|c_{ni}|^2$, hence the sign (or phase) of the coupling is not important and the fluctuations are strictly Gaussian. A different situation is in the case when the coupling is nonlinear [51–53] and the statistics is then not Gaussian [33,34,54]. Even for a harmonic bath in excitonic aggregates, intermolecular resonant couplings lead to shifts of phonon energies in their excited states and hence emergence of non-Gaussian statistics [55,56]. The emergence of interpigment correlations (when the bath is nonlocal) [57,58] in their excited states is yet another component which may lead to non-Gaussian statistics making the sign of the c_{ni} parameter important for realistic simulations. However, this property is not the main focus in this paper. In this paper, c_{ni} coupling constants are defined up to a sign.

Couplings to all of the relevant phonons are convenient to describe using integral quantity such as the spectral density. Mathematically, it comes from the antisymmetric part of the Fourier-transformed equilibrium fluctuation correlation function. In general, the correlation function is defined in the Heisenberg representation as

$$C_{kl,mn}(t) = \text{Tr}([\hat{H}_{\text{SB}}(t)]_{kl}[\hat{H}_{\text{SB}}(0)]_{mn}\sigma_T). \tag{7}$$

Here $\sigma_T = Z^{-1}\exp(-\beta\hat{H}_B)$ is the bath equilibrium density matrix; Z being the partition function, while

$$\hat{H}_{\text{SB}}(t) = -\sum_{ni} c_{ni}|n\rangle\langle n|(\hat{a}_i^\dagger e^{i\omega_i t} + \hat{a}_i e^{-i\omega_i t}). \tag{8}$$

In the above Hamiltonian, only diagonal electronic elements fluctuate and it is often assumed that fluctuations of different molecules are independent (local bath model). This is a rough approximation for intermolecular vibrations, while it is often the case for intramolecular vibrations. Technically, in the above $\hat{H}_{\text{SB}}(t)$ Hamiltonian, different molecules are coupled to their unique set of oscillators, so c_{ni} can be partitioned into specific nonzero blocks related to specific molecules. The correlation function then has only a few elements $C_{nn,nn}(t)$, which can be written using the spectral densities:

$$C_{nn,nn}(t) = \int_{-\infty}^{\infty}\frac{d\omega}{2\pi}\mathcal{G}(\omega,t)C''_n(\omega), \tag{9}$$

where

$$\mathcal{G}(\omega,t) = \coth\left(\frac{\beta\omega}{2}\right)\cos(\omega t) - i\sin(\omega t) \tag{10}$$

is the dimensionless thermal phonon Green's function, while the spectral density follows from the coupling pattern defined

above:

$$C_n''(\omega) = \pi \sum_j c_{nj}^2 [\delta(\omega - \omega_j) - \delta(\omega + \omega_j)], \tag{11}$$

where the summation is only over phonons associated with nth molecule. The reorganization energy is then given by

$$\Lambda_n = \int_0^\infty \frac{d\omega}{\pi} \frac{C_n''(\omega)}{\omega}. \tag{12}$$

Often a continuous spectral density function is used, such as Drude or the Ohmic model, while a log-normal function well approximates realistic phonons of protein bath [50,59].

The above model allows formulating the fluctuating exciton model, which is obtained by using the eigenstates of the system Hamiltonian:

$$\sum_n J_{mn} \psi_{ne} = \varepsilon_e \psi_{me}. \tag{13}$$

Then the whole Hamiltonian is transformed into the exciton picture $\hat{H}^{(\mathrm{exc})} = \psi^\dagger \hat{H} \psi$. The electronic Hamiltonian becomes diagonal, while the fluctuating part is not zero for all Hamiltonian elements

$$\hat{H}^{(\mathrm{exc})} = \sum_e \varepsilon_e |e\rangle\langle e| + \sum_i \omega_i (\hat{a}_i^\dagger \hat{a}_i + 1/2) - \sum_{ee'} |e'\rangle\langle e| \left(\sum_i c_{e'e,i}^{(\mathrm{exc})} (\hat{a}_i^\dagger + \hat{a}_i) \right). \tag{14}$$

Here $|e\rangle$ are exciton eigenstates with $\langle n|e\rangle = \psi_{ne}$ and

$$c_{e'e,i}^{(\mathrm{exc})} = \sum_n c_{ni} \psi_{ne'} \psi_{ne}. \tag{15}$$

Still, the system-bath model is bilinear, however, the fluctuations are now delocalized and correlated between different matrix elements, while the degree of delocalization depends on the system Hamiltonian matrix J. Often a delocalization measure for an exciton is introduced as the inverse participation ratio:

$$L_e^{(\mathrm{ipr})} = \frac{1}{\sum_n \psi_{ne}^4}. \tag{16}$$

Alternatively, the density-matrix based localization length includes dynamic incoherent localization of mixed states [38]:

$$L_e^{(dm)} = 1 + \sum_{mn}^{m \neq n} |\rho_{mn}|, \tag{17}$$

where ρ_{mn} is the density matrix of the electronic subsystem. In both cases, delocalization parameters have values between 1 for completely localized states and N, the number of molecules in the system, for completely delocalized excitons.

III. DYNAMIC MODELS FOR EXCITONS USING HEISENBERG PICTURE

Exciton-phonon dynamics equations can be obtained by using Heisenberg equations of motion in the Heisenberg picture, which is flexible in spectroscopy simulations of the excitons and their scattering in molecular aggregates [60–66]. The Heisenberg equation approach has also been developed for the semiconductor nonlinear response for calculation of electron-hole correlated optical excitations. Since the optical excitation is the source of electron and hole creation and annihilation, the hierarchy of many-body density matrices for a pair-conserving many-electron model is rigorously truncated to a given order in the radiation field. At third order to the optical field, up to five distinct equations are obtained similar to semiconductor Bloch equations. The approach allows for the analysis of the interplay between coherent and incoherent dynamics including many-body correlations. The approach is formally equivalent for semiconductors and for Frenkel excitons [63,64,67].

The approach relies on the well-known Heisenberg equation:

$$\frac{d\hat{O}}{dt} = i[\hat{H}, \hat{O}], \tag{18}$$

where $\hat{O}$ is an arbitrary operator. Its expectation value $O(t) = \langle \hat{O}(t) \rangle$ then can be calculated at an arbitrary time given the initial wave function, $\langle \hat{O}(t) \rangle = \langle \psi(t_0) | \hat{O}(t - t_0) | \psi(t_0) \rangle$. Since our complete description defines the system and bath in the same combined wave function, defining initial states for both the system and bath degrees of freedom allows us to calculate expectation values at an arbitrary later time.

The Hamiltonian in Eq. (6) is written in terms of the electronic projection operators using bra-ket notation $|m\rangle\langle n|$ within the single-exciton manifold and the phonon creation and annihilation operators, $\hat{a}_j^\dagger$ and $\hat{a}_j$. Therefore, for electronic degrees of freedom, it is convenient to focus on the electronic projection operator. To proceed, we thus explicitly define the operator

$$\hat{\pi}_{kl} = |k\rangle\langle l|. \tag{19}$$

The important property of the projector is that its product with another projection operator is yet another projection operator:

$$\hat{\pi}_{ij} \hat{\pi}_{kl} = |i\rangle\langle j|k\rangle\langle l| = \delta_{jk} \hat{\pi}_{il}, \tag{20}$$

and since the whole Hamiltonian is written in terms of such operators, the time evolution with this Hamiltonian does not generate different types of operators. This allows us to develop the set of equations where the specific multiplications of excitations is not explicitly counted, which is very convenient for exciton-phonon coupled dynamics. This is, of course, restricted to our choice of the Hamiltonian and the set of phenomena we are interested in, which are within the single exciton manifold. Also, note that the whole set of electronic projection operators denotes the system density operator $\hat{\rho} = \sum_{kl} \hat{\pi}_{lk}$, which allows calculating required expectation values. Then, for the phonon degrees of freedom we use the phonon creation and annihilation operators, $\hat{a}_j^\dagger$ and $\hat{a}_j$.

It has been mentioned above that the Heisenberg equation approach has been used for optical response (spectroscopy signals) simulations. It is important to note that the optical response is mostly related to excitation and deexcitation of the materials, hence creation and annihilation of excitons in molecular systems or electrons and holes in semiconductors (in terms of the corresponding operators). Hence, the number of excitations can be explicitly followed in equations and can be associated to the order of optical response.

For example, up to two excitons (two electron-hole pairs) are involved in resonant third order optical response. This ordering results in a specific number of coupled equations for the given order of optical response [67,68]. In this paper, we consider only singly excited molecular systems, hence only the single excitation manifold is considered and the creation and annihilation of the excitons is not followed explicitly. The main focus is related to intraband exciton phonon processes as the Hamiltonian without optical field conserves the number of excitons. On the other hand, the number of phonons varies because of exciton relaxation and this is the cause of equation hierarchy as described for semiconductors in Ref. [68].

The Heisenberg equation requires calculating various electronic commutators:

$$[\hat{H}_S, \hat{\pi}_{kl}] = \sum_n (J_{nk}\hat{\pi}_{nl} - J_{ln}\hat{\pi}_{kn}), \tag{21}$$

$$[\hat{H}_B, \hat{\pi}_{kl}] = 0, \tag{22}$$

$$[\hat{H}_{\rm SB}, \hat{\pi}_{kl}] = \sum_j (c_{lj} - c_{kj})(\hat{a}_j + \hat{a}_j^\dagger)\hat{\pi}_{kl}. \tag{23}$$

The next set of commutators is for phonon operators. Then $[\hat{H}_S, \hat{a}_i] = 0$,

$$[\hat{H}_B, \hat{a}_i] = -\omega_i \hat{a}_i, \tag{24}$$

$$[\hat{H}_{\rm SB}, \hat{a}_i] = \sum_n c_{ni}\hat{\pi}_{nn}. \tag{25}$$

All other commutators are zero.

Using these commutators, equations of motion are easily obtained. For example, for a phonon we primarily find

$$-i\frac{d\hat{a}_j}{dt} = -\omega_j \hat{a}_j + \sum_n c_{nj}\hat{\pi}_{nn}. \tag{26}$$

While this is an abstract equation for an operator, the equations capture a specific physical concept: the response of a phonon to the population of the site where the nonzero population $\pi_{nn} = \langle \hat{\pi}_{nn} \rangle$ induces the phonon creation and annihilation. In the following, we use letters without hats to denote expectation values, i.e., $\langle \hat{a}_j \rangle \equiv a_j$.

However, the main observable is the population and the electronic density operator. Also notice that the normalization condition requires

$$\sum_n \pi_{nn} = 1 \tag{27}$$

and $\pi_{kl}^2 \leqslant \pi_{kk}\pi_{ll}$, where the equal sign corresponds to the pure state, while "$<$" is for the mixed state. We can then write the equation for the projector

$$-i\frac{d\hat{\pi}_{kl}}{dt} = \sum_n (J_{nk}\hat{\pi}_{nl} - J_{ln}\hat{\pi}_{kn}) - \sum_j (c_{kj} - c_{lj})(\hat{a}_j\hat{\pi}_{kl} + \hat{a}_j^\dagger\hat{\pi}_{kl}). \tag{28}$$

The two equations (26) and (28) then generate all remaining equations—on the right-hand side in Eq. (28), we find products $\hat{a}_j\hat{\pi}_{kl}$ and $\hat{a}_j^\dagger\hat{\pi}_{kl}$, which require their own equations. For example,

$$-i\frac{d\hat{a}_j\hat{\pi}_{kl}}{dt} = -\omega_\alpha \hat{a}_j\hat{\pi}_{kl} + \sum_n (J_{nk}\hat{a}_j\hat{\pi}_{nl} - J_{ln}\hat{a}_j\hat{\pi}_{kn}) - \sum_i (c_{ki} - c_{li})(\hat{a}_i^\dagger\hat{a}_j\hat{\pi}_{kl} + \hat{a}_j\hat{a}_i\hat{\pi}_{kl}) + c_{lj}\hat{\pi}_{kl}. \tag{29}$$

In addition, $\hat{a}_j^\dagger\hat{\pi}_{kl} = (\hat{a}_j\hat{\pi}_{lk})^\dagger$, so the additional equation for the creation operator it is not necessary.

Equations for operators can be quickly updated to equations for expectation values using the properties of the Heisenberg picture. Specifying $t_0 = 0$ and when the state at this time is fully defined, the expectation values then satisfy the same equations of motion

$$-i\frac{da_j}{dt} = -\omega_j a_j + \sum_n c_{nj}\pi_{nn}, \tag{30}$$

$$-i\frac{d\pi_{kl}}{dt} = \sum_n (J_{nk}\pi_{nl} - J_{ln}\pi_{kn}) - \sum_j (c_{kj} - c_{lj})(\overline{a_j\pi_{kl}} + \overline{a_j^*\pi_{kl}}), \tag{31}$$

where for the composite variables we denote $\overline{a_j\pi_{kl}} = \langle \hat{a}_j\hat{\pi}_{kl} \rangle$; and $\overline{a_j^*\pi_{kl}} = \langle \hat{a}_j^\dagger\hat{\pi}_{kl} \rangle$. Then, according to Eq. (29), we generate higher level variables: $\overline{a_ia_j\pi_{kl}} = \langle \hat{a}_i\hat{a}_j\hat{\pi}_{kl} \rangle$ and similarly for the variables with conjugate operators.

On the right-hand side, we generate new combinations of operators of growing number of phonon operators. Then we should write equations for these products and that would generate an infinite hierarchy of excitonic-vibronic equations. All equations can be combined into a single equation:

$$\begin{aligned}
&-i\frac{d\overline{a_{j_K}^*\ldots a_{j_1}^* a_{i_L}\ldots a_{i_1}\pi_{kl}}}{dt} \\
&= \sum_n (J_{nk}\overline{a_{j_K}^*\ldots a_{i_1}\pi_{nl}} - J_{ln}\overline{a_{j_K}^*\ldots a_{i_1}\pi_{kn}}) \\
&\quad - (\omega_{i_L} + \ldots + \omega_{i_1} - \omega_{j_K} - \ldots - \omega_{j_1})\overline{a_{j_K}^*\ldots a_{i_1}\pi_{kl}} \\
&\quad - \sum_s (c_{ks} - c_{ls})(\overline{a_s^* a_{j_K}^*\ldots a_{i_1}\pi_{kl}} + \overline{a_{j_K}^*\ldots a_{i_1}a_s\pi_{kl}}) \\
&\quad - \sum_s^{s=j_K\ldots j_1} c_{ks}\overline{a_{j_K}^*\ldots a_{s+1}^* a_{s-1}^*\ldots a_{j_1}^* a_{i_L}\ldots a_{i_1}\pi_{kl}} \\
&\quad + \sum_s^{s=i_L\ldots i_1} c_{ls}\overline{a_{j_K}^*\ldots a_{j_1}^* a_{i_L}\ldots a_{s+1}a_{s-1}\ldots a_{i_1}\pi_{kl}}.
\end{aligned} \tag{32}$$

This equation defines the complete vibronic model for the coupled exciton-phonon dynamics, where different reduced models can be formulated by performing various approximations. Most importantly, this equation can be applied for the coherent and incoherent case, i.e., when the system is either in a pure or mixed state.

A. Mean-field approximation

The mean field approximation (MFA) is defined by assuming an uncorrelated quantum description of exciton and

phonon dynamics. We thus have two coupled equations which define the closed excitonic system. The first equation is for the exciton density matrix,

$$-i\frac{d\pi_{kl}}{dt} = \sum_n (J_{nk}\pi_{nl} - J_{ln}\pi_{kn}) - (\xi_k(a) - \xi_l(a))\pi_{kl}, \tag{33}$$

and the other is for phonons:

$$-i\frac{da_i}{dt} = -\omega_i a_i + \sum_n c_{ni}\pi_{nn}. \tag{34}$$

Here $\xi_k(a) = \sum_i c_{ki}(a_i + a_i^*)$ is the real-value cumulative force acting on the exciton density matrix. The exciton and phonon subsystems act onto each other as the external fields, which corresponds to the mean-field-type description. This level of theory corresponds to a mixed quantum-classical model for wave-function evolution (similar averaged over fluctuations type of description is possible for density matrix as well in Ref. [20]). The same level description is denoted as coherent phonon approach in Ref. [68]. However, the variables are incoherently mixed at finite temperature, hence MFA term is more appropriate. The main idea behind the MFA approach is that essentially all quantum variables (such as π_{ij} and a_i) become affected by cumulative (fluctuating) forces as the classical fields [see Eqs. (33) and (34)].

MFA allows us to determine the polaron formation, assuming separation of timescales. For fixed populations and initial values $a_i(0) = 0$, the solution of the phonon equation is

$$a_i(t) = \sum_n \frac{c_{ni}}{\omega_i}\pi_{nn}(1 - e^{-i\omega_i t - \gamma t}); \tag{35}$$

here the rotation is around $\sum_n c_{ni}\pi_{nn}/\omega_i$, while $\gamma \ll \omega_i$ is the phenomenological damping. As the populations are affected by cumulative phonon field, asymptotically at $\gamma t \gg 1$ we explicitly find the exciton Hamiltonian deformation phenomena due to nonzero exciton population π_{nn}:

$$-i\frac{d\pi_{kl}}{dt} = \left(\sum_n^{n\neq k} J_{nk}\pi_{nl} - \sum_n^{n\neq l} J_{ln}\pi_{kn}\right) + (\bar{J}_{kk}(\pi) - \bar{J}_{ll}(\pi))\pi_{kl}, \tag{36}$$

where population-induced shifted site energies are

$$\bar{J}_{kk} = J_{kk} - 2\sum_{ni}\frac{c_{ki}c_{ni}}{\omega_i}\pi_{nn}. \tag{37}$$

This shift corresponds to phonon-induced deformation potential across the lattice. The presence of such deformation is the first manifestation of the polaron formation.

How can the polaron effect be quantified? One of the characteristics of an exciton is its extension or delocalization. Indeed, the electrons and holes in semiconductors as well as excitons in pure crystals are infinitely extended Bloch waves [69,70]. Deformation potential is then a source of exciton scattering and localization [38,71] and has been recently observed in, e.g., perovskites [72–74]. Finite-size realistic molecular aggregates experience reduced exciton size due to inhomogeneities of the materials, while extra localization comes from coupling to phonons [38,71]. Consider, for example, two coupled molecules (or simple lattice sites) with similar electronic excitation energies and local vibrations (one vibration per site). The electronic Hamiltonian can be represented by a matrix

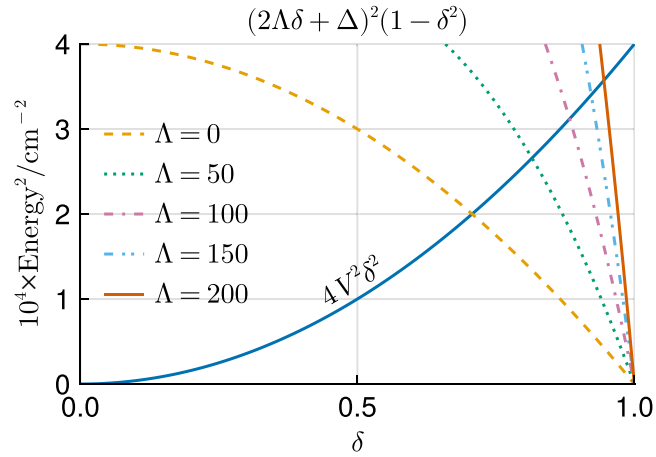


FIG. 1. Illustration of polaron formation [Eq. (41)] for different reorganization energies. Blue line: $4V^2\delta^2$, others: $(2\Lambda\delta + \Delta)^2(1 - \delta^2)$; here $J_{12} \equiv -V$ is the resonant coupling, Δ is the site energy difference, $\delta = \pi_{11} - \pi_{22}$ is the population difference. Parameters are $\Delta = 200\,\mathrm{cm}^{-1}$, $V = 100\,\mathrm{cm}^{-1}$. Λ is the reorganization energy. The crossing points are the stationary solutions. $\Lambda = 0$ case corresponds to the exciton model. Increase of the population difference δ up to 1 with increasing reorganization energy Λ is a direct manifestation of exciton localization (see main text).

$$H_S = \begin{pmatrix} J_{11} & J_{12} \\ J_{12} & J_{11} + \Delta \end{pmatrix}. \tag{38}$$

As an example, we take $J_{11} = \varepsilon$, $J_{22} = \varepsilon + 200\,\mathrm{cm}^{-1}$, while $J_{12} = J_{21} = -100\,\mathrm{cm}^{-1}$. When coupling to phonons is negligible, the stationary states of the system are exciton states. The lower state has energy $\varepsilon - 41.42\,\mathrm{cm}^{-1}$, with eigenvector

$$|\phi\rangle = \begin{pmatrix} 0.9238 \\ 0.3826 \end{pmatrix}. \tag{39}$$

The corresponding pure state density matrix is

$$\rho = \begin{pmatrix} 0.8535 & 0.3535 \\ 0.3535 & 0.1465 \end{pmatrix}. \tag{40}$$

The exciton's delocalization is $L^{(dm)} = 1.707$. The delocalization is less than 2 because of Hamiltonian asymmetry.

Next we include a single vibration per site, hence $c_{k\alpha}$ is diagonal with nonzero elements $c_{11} = c_{22}$ and $\omega_1 = \omega_2$. Stationary solution is defined by the mean field equations. Denoting $\pi_{11} + \pi_{22} = 1$, $\pi_{11} - \pi_{22} = \delta$, at pure state ($\pi_{12}^2 = \pi_{11}\pi_{22}$), we find fourth order equation for populations:

$$4V^2\delta^2 = (2\Lambda\delta + \Delta)^2(1 - \delta^2). \tag{41}$$

Here $J_{12} \equiv -V$ is the resonant coupling, $\Delta = J_{22} - J_{11}$ is the electronic energy difference, and $\Lambda = c_{11}^2/\omega_1$ is the reorganization energy. The solution of this fourth order equation is possible to illustrate graphically as shown in Fig. 1, where on the horizontal axis we have the population difference

δ, while on the vertical axis we plot functions $4V^2\delta^2$ and $(2\Lambda\delta+\Delta)^2(1-\delta^2)$ for the above-defined dimer model. The solutions for the equation are the points where the curves intersect. The figure demonstrates changes of the stationary population difference with increasing reorganization energy. Indeed, for larger Λ values, the intersection point shifts toward larger exciton population difference δ. Notice that the population difference can be related to exciton delocalization as $L^{(dm)} = 1 + 2|\pi_{12}| = 1 + \sqrt{1-\delta^2}$, so as population difference ρ increases the delocalization length decreases; hence for reorganization energy $200\,\mathrm{cm}^{-1}$ we find $\delta \approx 0.9$ and the delocalization decreases down to $\sim$1.5. The complete localization would correspond to $\delta = 1$, i.e., $\pi_{11} = 1, \pi_{22} = 0$.

The polaron formation is well described by this level of theory, however, spectroscopic properties in semiclassical approximation fail to properly describe thermally induced phonon sidebands in absorption as will be demonstrated in the Sec. V.

B. Optical absorption

Simple spectroscopic measurements, such as absorption, depend only on single-excitation block of states. It is then convenient to define the isolated ground state $|g\rangle$, where all quantities are defined with respect to that state; hence the ground state has zero coupling to the phonons and to the other electronic states. This state is coupled to other states only via the system-field interaction. In the dipole approximation in Schroedinger representation, this interaction corresponds to an additional term in the full Hamiltonian:

$$\hat{H}_{SF} = -\sum_{n}^{\mathrm{exc}} \hat{\pi}_{gn}\boldsymbol{\mu}_{gn}\cdot\boldsymbol{\mathcal{E}}^{(-)}(t) + \mathrm{H.c.} \tag{42}$$

The summation is only over the excited states. Here $\boldsymbol{\mathcal{E}}^{(-)}(t) \sim \exp(-i\omega_0 t)$ is the optical field within the rotating wave approximation (RWA), H.c. denotes hermitian conjugate, while $\boldsymbol{\mu}_{gn}$ is the transition dipole. The induced polarization, which is necessary for optical responses in Heisenberg representation is then given by

$$P(t) = \sum_{n}^{\mathrm{exc}} \pi_{gn}(t)\boldsymbol{\mu}_{gn} + \mathrm{c.c.} \tag{43}$$

The linear absorption spectrum is given by Fourier transform of the first order induced polarization for a short excitation pulse, i.e., when $\boldsymbol{\mathcal{E}}(t)$ is a short (Gaussian) infinitesimally weak pulse centered at zero time:

$$\kappa(\omega) = \int_{-\infty}^{\infty} dt e^{i\omega t} P(t). \tag{44}$$

If the system is in the ground state before excitation with probability 1, only $\pi_{gn}(t)$ coherence is induced by the weak optical pulse. The first order equations in the MFA for $\pi_{gk}(t)$ coherence are as follows:

$$-i\frac{d\pi_{gk}}{dt} = -\sum_{n}^{\mathrm{exc}} J_{kn}\pi_{gn} + \sum_{j} c_{kj}(a_j + a_j^*)\pi_{gk} + \mu_{gk}\mathcal{E}^{(-)}(t), \tag{45}$$

and the equation has to be supplemented by zero order equation for phonons:

$$-i\frac{da_j}{dt} = -\omega_j a_j. \tag{46}$$

Solving the last equation $a_j(t) = \exp(-i\omega_j t)a_{j0}$, where a_{j0} is the initial thermal fluctuation value, we can simplify

$$-i\frac{d\pi_{gk}}{dt} = -\sum_{n}^{\mathrm{exc}} J_{kn}\pi_{gn} + \pi_{gk}\xi_k(t) + \mu_{gk}\mathcal{E}(t), \tag{47}$$

where now

$$\xi_l(t) = 2R\sum_{\alpha} c_{l\alpha}a_{\alpha 0}e^{-i\omega_\alpha t} \tag{48}$$

describes the classical thermal noise. We find that π_{gk} determines the main excitonic peaks, while a_j induces classical thermal fluctuations. These equations thus include absorption thermal broadening via bath fluctuations and fluctuations are from classical oscillators. However, as the classical noise is Gaussian, the resulting line broadening is symmetric, which does not capture correct temperature behavior at low temperature (e.g., zero-temperature phonon sidebands).

The model becomes more complicated at a one step higher level, which we denote by one quantum approximation (1QA). Here we include first order correlations between exciton and phonon variables. The following three equations describe the optical coherence:

$$-i\frac{d\pi_{gl}}{dt} = -\sum_{n} J_{ln}\pi_{gn}(t) + \mu_{gl}\mathcal{E}^{(-)}(t) + \sum_{j} c_{lj}(\overline{a_j^*\pi_{gl}}(t) + \overline{a_j\pi_{gl}}(t)) \tag{49}$$

$$-i\frac{d\overline{a_j\pi_{gl}}}{dt} = -\omega_j\overline{a_j\pi_{gl}}(t) - \sum_{n} J_{ln}\overline{a_j\pi_{gn}}(t) + a_j(t)\mu_{gl}\mathcal{E}^{(-)}(t) + (\xi_l(t)a_j(t) + c_{lj})\pi_{gl}(t), \tag{50}$$

$$-i\frac{d\overline{a_j^*\pi_{gl}}}{dt} = \omega_j\overline{a_j^*\pi_{gl}}(t) - \sum_{n} J_{ln}\overline{a_j^*\pi_{gn}}(t) + a_j^*(t)\mu_{gl}\mathcal{E}^{(-)}(t) + \xi_l(t)a_j^*(t)\pi_{gl}(t). \tag{51}$$

Here we keep variables $\overline{a_j\pi_{kl}}$ and $\overline{a_j^*\pi_{kl}}$ unfactorized, but the higher order system-bath coupling terms are factorized as in MFA: $\overline{a_j^*a_i\pi_{gl}} = a_j^*a_i\pi_{gl}^{(1)}$ and $\overline{a_ja_i\pi_{gl}}^{(1)} = a_ja_i\pi_{gl}^{(1)}$.

Notice that in our approach in 1QA, up to one phonon states are treated as quantum variables, however, the higher order excitations are treated again within the MFA. Since MFA approximation leads to classical fluctuating phonon field description, 1QA becomes a mixed quantum-classical description, where at small phonon populations the approach includes them as quantum particles, while at high phonon excitations, the classical phonon field dominates. Such approach, in principle, is more relevant than the pure quantum one-particle model [75], where more than single phonon quanta excitations are completely ignored. This computational simplification allows for significant reduction of the computational cost [76–78]. However, it may lead to incorrect absorption spectra when excitonic resonances match phonon

frequencies, and when the number of phonon excitations is large [55].

Again, for absorption purposes the phonon variables $a_j(t)$ can be taken at zero order, $a_j(t) = \exp(-i\omega_j t)a_{j0}$. As it comes from equations, variables $\overline{a_i \pi_{gl}}$ and $\overline{a_i^* \pi_{gl}}$ are affected by classical thermal noise $\xi_l(t)$, however, they are not affected identically, thus the net fluctuations of optical coherence π_{gl} are not symmetric as it was in MFA. We find that while π_{gl} determines the main excitonic peaks, $\overline{a_j \pi_{gl}}$ determines additional phonon-induced peaks at higher (and lower) energies than the main electronic transitions even at zero temperature. The theory thus should correctly represent one-phonon level sidebands.

The full unfactorized 1QA set of equations are presented in Appendix A. When excitation is perturbative, the total thermal equilibrium with respect to the ground state can be accepted. Then these equations lead to the well-known Redfield relaxation expression.

However, the 1QA equations as well as MFA equations are formulated beyond this restriction and can describe the nonlinear effects such as polaron formation, which is not reflected in absorption or in Redfield relaxation. The next section is devoted to describing such properties.

IV. EXCITATION EVOLUTION IN POLARON REPRESENTATION

The above-defined Hamiltonian is written with respect to the electronic ground state. Accordingly, all the degrees of freedom in electronic ground states are independent. In the electronic excited state, the phonon equilibrium is shifted, which changes the symmetry of electronic excitations: if site n is excited, the phonons, which are coupled to the nth site, find new equilibrium $d_{ni} = \sqrt{2}c_{ni}/\omega_i$. This shifts down the nth excited state energy by reorganization energy Λ_n, while the transition energy is shifted by $2\Lambda_n$. It thus may be more convenient to work in another set of coordinates, which are centered around zero (or somewhere in between the ground and excited state equilibria) in the electronic excited state. A polaron transformation can be used to include this change [79,80].

The polaron unitary transformation is defined for an arbitrary operator by

$$\exp(\hat{G})\hat{O}\exp(-\hat{G}) \to \hat{O}' \tag{52}$$

using the generating operator

$$\hat{G}^{(p)} = -\sum_{ni} \frac{c_{ni}}{\omega_i}(\hat{a}_i^\dagger - \hat{a}_i)|n\rangle\langle n|. \tag{53}$$

This implies a shift of the phonon, depending on the state of the molecule. However, some phonons, which are weakly coupled to the excitations, may be better described with respect to the electronic ground state. To include this freedom, we follow the partial polaron transformation description [22]. It introduces an additional weight factor:

$$\hat{G} = -\sum_{ni} w_i \frac{c_{ni}}{\omega_i}(\hat{a}_i^\dagger - \hat{a}_i)|n\rangle\langle n|, \tag{54}$$

where $0 < w_i < 1$ is a variable weight factor, which can be tuned to control the transform. Notice that the unitary operator $\exp(\pm\hat{G})$ can be written as a shift operator [see Eq. (B11) in Appendix B]. Then the transformation can be written simply as

$$\hat{\mathcal{D}}^\dagger \hat{O}\hat{\mathcal{D}} \to \hat{O}', \tag{55}$$

where we use a multidimensional shift

$$\hat{\mathcal{D}} = \sum_n |n\rangle\langle n|\hat{D}(\boldsymbol{g}_n)$$

with the components $g_{ni} = w_i c_{ni}/\omega_i$. Note that $\hat{x} = (\hat{a}^\dagger + \hat{a})/\sqrt{2}$, so a coordinated shift by $\sqrt{2}c_{ni}/\omega_i$ corresponds to a shift of a_i by c_{ni}/ω_i. Using the identities of Appendix B, the transformed Hamiltonian can be calculated easily and yields the following relations:

$$\hat{\mathcal{D}}^\dagger \hat{H}_S \hat{\mathcal{D}} = \sum_{mn} |m\rangle\langle n|J_{mn}\phi_{mn}(\hat{a}), \tag{56}$$

where

$$\phi_{mn}(\hat{a}) = \hat{D}(\boldsymbol{g}_n - \boldsymbol{g}_m). \tag{57}$$

Then

$$\hat{\mathcal{D}}^\dagger \hat{H}_B \hat{\mathcal{D}} = \hat{H}_B + \sum_n |n\rangle\langle n| \sum_i \left(\omega_i g_{ni}(\hat{a}_i + \hat{a}_i^\dagger) + \omega_i g_{ni}^2\right), \tag{58}$$

and, finally,

$$\hat{\mathcal{D}}^\dagger \hat{H}_{\mathrm{SB}} \hat{\mathcal{D}} = \hat{H}_{\mathrm{SB}} - 2\sum_n |n\rangle\langle n| \sum_i g_{ni}c_{ni}. \tag{59}$$

As a result, the transformed Hamiltonian can be written using the following partitioning into the system part and the system-bath coupling:

$$\hat{\tilde{H}} = \hat{\tilde{H}}_S + \hat{H}_B + \hat{\tilde{H}}_{\mathrm{SB}}. \tag{60}$$

The system Hamiltonian contains only the diagonal part:

$$\hat{\tilde{H}}_S = \sum_n |n\rangle\langle n|\tilde{J}_{nn}, \tag{61}$$

with the renormalized energies

$$\tilde{J}_{nn} = J_{nn} - \sum_i (2 - w_i)g_{ni}c_{ni}, \tag{62}$$

then the bath Hamiltonian stays the same and the system-bath coupling contains normalized electronic coupling fluctuations and tuned excitation energy fluctuations:

$$\tilde{H}_{\mathrm{SB}} = \sum_{mn}^{m\neq n} |m\rangle\langle n|J_{mn}\phi_{mn}(\hat{a}) - \sum_n |n\rangle\langle n| \sum_i (1 - w_i)c_{ni}(\hat{a}_i + \hat{a}_i^\dagger). \tag{63}$$

The resulting Hamiltonian becomes straightforward to characterize. Setting $w_i = 1$, we have the full polaron transformation, where the site energies are shifted, while intersite couplings are tuned by the bath. Setting $w_i = 0$ switches off the transformation completely. So, parameter w_i should be tuned so the polaron transformation is enabled for specific modes, which relax during the excitation evolution, while

the polaron transformation should be avoided for the modes, which do not relax.

A similar variational polaron transformation has been applied with an additional basis optimization involving the Bogoliubov's theorem [79] to characterize the crossover from bandlike transport to hopping transport in molecular crystals. The theorem allows us to easily estimate the temperature-dependent thermal energy. Hence, taking the extremum of this energy can be used to fix the transformation weight coefficients. The obtained result indicates that the optimal polaron theory can describe the charge-carrier mobilities quantitatively across the whole experimental temperature range in molecular crystals.

The system-bath coupling fluctuations at thermal equilibrium in polaron representation in the electronic ground state do not average to zero. To characterize the extent of fluctuations, it may be convenient to separate fluctuating part from the average Hamiltonian to evaluate the effect of transformation on the fluctuation amplitude. This can be accounted by shifting the Hamiltonian with respect to the thermal equilibrium. Let us partition the Hamiltonian as follows:

$$\hat{H} = \hat{H}_0 + \hat{H}', \tag{64}$$

where

$$\hat{H}_0 = \hat{\tilde{H}}_S + H_B + \langle \hat{\tilde{H}}_{\rm SB} \rangle_T \tag{65}$$

and

$$\hat{H}' = \hat{\tilde{H}}_{\rm SB} - \langle \hat{\tilde{H}}_{\rm SB} \rangle_T. \tag{66}$$

Here

$$\langle \hat{\tilde{H}}_{\rm SB} \rangle_T = Tr_B[\hat{\tilde{H}}_{\rm SB} \sigma_T] \tag{67}$$

is the temperature-dependent mean value with respect to the bath equilibrium density operator. The last expression can be explicitly calculated by expanding the $\langle \tilde{H}_{\rm SB} \rangle_T$ in harmonic oscillator basis states, which leads to

$$\langle \tilde{H}_{\rm SB} \rangle_T = \sum_{mn}^{m \neq n} |m\rangle\langle n| \tilde{J}_{mn}, \tag{68}$$

where for the local bath

$$\tilde{J}_{mn} = J_{mn} \exp\left(-\frac{1}{2} \sum_i (g_{ni} - g_{mi})^2 \coth\left(\frac{\beta \omega_i}{2} \right) \right); \; m \neq n \tag{69}$$

is the renormalized temperature-dependent resonant coupling.

The resulting system Hamiltonian $\hat{H}_0$ thus contains downshifted site energies [Eq. (62)], $\tilde{J}_{nn}$, reduced couplings [Eq. (69)] $\tilde{J}_{mn}$, while system-bath coupling $\hat{H}'$ becomes exponential for the couplings and linear for the transition energies:

$$\hat{H}_0 = \sum_{mn} |m\rangle\langle n| \tilde{J}_{mn} + H_B, \tag{70}$$

$$\tilde{H}' = \sum_{mn}^{m \neq n} |m\rangle\langle n| (J_{mn} \phi_{mn}(\hat{a}) - \tilde{J}_{mn}) - \sum_n |n\rangle\langle n| \sum_i (1 - w_i) c_{ni} (\hat{a}_i + \hat{a}_i^\dagger). \tag{71}$$

Using this set of equations, we can define the polaronic excited states, given by eigenequation

$$\tilde{J}_{nn} \varphi_{np} + \sum_m^{m \neq n} \tilde{J}_{nm} \varphi_{mp} = \tilde{\varepsilon}_p \varphi_{np}. \tag{72}$$

The corresponding full Hamiltonian in the polaron representation is then

$$\hat{H}^{(\rm pol)} = \sum_p \tilde{\varepsilon}_p |p\rangle\langle p| + \sum_i \omega_i (\hat{a}_i^\dagger \hat{a}_i + 1/2) + \sum_{pp'} |p'\rangle\langle p| \left(X^{(\rm pol)}_{p'p}(\hat{a}) - Y^{(\rm pol)}_{p'p}(\hat{a}) \right), \tag{73}$$

while it contains more complicated system-bath coupling with the fluctuating terms

$$X^{(\rm pol)}_{p'p}(\hat{a}) = \sum_{mn}^{m \neq n} \varphi^*_{mp'} \varphi_{np} (J_{mn} \phi_{mn}(\hat{a}) - \tilde{J}_{mn}) \tag{74}$$

and

$$Y^{(\rm pol)}_{p'p}(\hat{a}) = \sum_i \sum_n \varphi^*_{np'} \varphi_{np} c_{ni} (1 - w_i)(\hat{a}_i + \hat{a}_i^\dagger). \tag{75}$$

Still, the system-bath coupling is zero at thermal bath equilibrium, and thus similar to exciton model yields only thermal fluctuations. However, the whole purpose of the transformation is to obtain smaller fluctuation amplitudes. Tuning parameter w_i, one can switch to the exciton model with $w_i = 0$ when $X^{(\rm pol)}(\hat{a}) = 0$ and to full polaron model with $w_i = 1$ when $Y^{(\rm pol)}(\hat{a}) = 0$. However, the intermediate case may be most efficient since then the system-bath fluctuations can be minimized.

The magnitude of fluctuations is estimated via the correlation functions in the Heisenberg representation:

$$C_{p_4 p_3, p_2 p_1}(t) = {\rm Tr}_B[\tilde{H}'(t) \tilde{H}'(0) \sigma_B(T)]. \tag{76}$$

In the present case, due to the specific form of the system-bath coupling, the three types of correlation functions describe the magnitude of fluctuations:

$$C_{p_4 p_3, p_2 p_1}(t) = \langle XX \rangle^{(\rm pol)}_{p_4 p_3, p_2 p_1}(t) + \langle XY \rangle^{(\rm pol)}_{p_4 p_3, p_2 p_1}(t) + \langle XY \rangle^{(\rm pol)}_{p_2 p_1, p_4 p_3}(-t) + \langle YY \rangle^{(\rm pol)}_{p_4 p_3, p_2 p_1}(t). \tag{77}$$

The expressions for them for the local bath are

$$\langle XX \rangle^{(\rm pol)}_{p_4 p_3, p_2 p_1}(t) = \sum_{mn}^{m \neq n} \sum_{m'n'}^{m' \neq n'} \varphi^*_{mp_4} \varphi_{np_3} \varphi^*_{m'p_2} \varphi_{n'p_1} \tilde{J}_{mn} \tilde{J}_{m'n'} \left(\exp\left(-\frac{1}{2} \sum_j f_{mnj} f_{m'n'j} \mathcal{G}(\omega_j, t) \right) - 1 \right), \tag{78}$$

$$\langle YY\rangle^{(\mathrm{pol})}_{p_4p_3,p_2p_1}(t)=\sum_n \varphi^*_{np_4}\varphi_{np_3}\varphi^*_{np_2}\varphi_{np_1}\sum_j c^2_{nj}(1-w_j)^2\mathcal{G}(\omega_j,t), \tag{79}$$

$$\langle XY\rangle^{(\mathrm{pol})}_{p_4p_3,p_2p_1}(t)=i\sum_{mn}^{m\neq n}\varphi^*_{mp_4}\varphi_{np_3}J_{mn}\sum_j \frac{w_j(1-w_j)}{\omega_j}\partial_t\mathcal{G}(\omega_j,t)\left(\varphi^*_{np_2}\varphi_{np_1}c^2_{nj}-\varphi^*_{mp_2}\varphi_{mp_1}c^2_{mj}\right). \tag{80}$$

As the time dependence of these functions is similar, it is sufficient to consider the zero time case, where $\mathcal{G}(\omega,t=0)=\coth(\beta\omega/2)$ and $\partial_t\mathcal{G}(\omega,t=0)=-i$.

Notice that these functions completely describe the dynamics of the reduced exciton-phonon dynamics in non-Markovian regime as shown in Ref. [22]. As fluctuating variables happen to be in exponentials, the fluctuations are not Gaussian and the exact dynamics cannot be completely represented by simple coordinate-coordinate correlation functions as in Redfield relaxation theory [81]. Moreover, the fluctuation correlation functions do not come explicitly if numerical propagation of the Heisenberg equations is employed. However, they have analytical expressions and can be used for evaluating the magnitude of fluctuations in the original representation and the transformed representation. The optimal set of weight coefficients can be chosen based on minimization of fluctuation amplitude in the original or in the transformed basis.

The polaron transformation also requires transforming all observable operators. An arbitrary expectation value is given by standard expression $A=\langle\Psi|\hat{A}|\Psi\rangle$ when all variables, i.e., the wave function and the operator corresponds to the specific representation. It is thus necessary to transform all relevant system operators. Such is, for example, the system projection operator, given by

$$\hat{\pi}^{(\mathrm{pol})}_{mn}=\hat{\pi}_{mn}\phi_{mn}(\hat{a}). \tag{81}$$

The operator thus shifts all the phonon operators due to $\phi_{mn}(\hat{a})$, which is relevant, for example, for a polarization operator in absorption calculation as shown below. Additionally, excitation evolution is necessary to evaluate for various applications. This could be realized by performing transformations for exciton evolution operators. However, the final result would be identical to the evolution of the original exciton model if no approximation is performed. Below we describe an approximate variational theory for modeling evolution of either excitons or polarons in the unified description.

A. Variational approach for generalized polaron model

Typically, the exciton Hamiltonian is used for describing the exciton relaxation. It can be nicely correlated to experimental conditions, where an initial state immediately after optical excitation (the pure exciton state) is well defined as the exciton state. However, on the longer times the excitons become dressed with phonons, so polaron description may be advantageous and more accurate. Here we take the generalized polaron Hamiltonian as the starting point. Having the polaronic model, the straightforward approach could be to write the Heisenberg equation of motion using the above described theory. However, the polaronic Hamiltonian contains exponentials of phonon operators and thus obtaining the operator equations is not so straightforward as in the exciton picture.

The variational approach is an alternative convenient method for describing the vibronic characteristics of the molecular systems. The starting point is the definition of a specific parameterized complete wave function, which will be written as a direct product of electronic excitation and a phonon subsystem:

$$\Psi(t)=\left(\sum_n \varphi_n(t)|n\rangle\right)\left(\prod_i|\alpha_i(t)\rangle\right). \tag{82}$$

Here φ_n is the electronic excitation amplitude on molecule n, $|\alpha_i(t)\rangle$ is a specific parameterized state of phonon i. One of the choices is to use the superposition of the phonon number states, what leads to time-dependent Hartree equations; the other choice is to use coherent states of the oscillator, which satisfy $\hat{a}_i|\alpha_i(t)\rangle=\alpha_i(t)|\alpha_i(t)\rangle$ (see Appendix B) [81]. Now the parameters of the wave function are amplitudes $\varphi_n(t)$ and $\alpha_i(t)$. Electronic excitation amplitudes satisfy normalization $|\varphi_n(t)|\leqslant 1$, while $\alpha_i(t)$ are arbitrary complex numbers having properties $q_i(t)\sim R\alpha_i(t)$, $p_i(t)\sim \mathrm{Im}\alpha_i(t)$.

Having the form of the wave function and the Hamiltonian, we can then use the quantum Lagrangian

$$\mathcal{L}=\frac{i}{2}\left(\left\langle\Psi(t)\middle|\frac{d\Psi(t)}{dt}\right\rangle-\left\langle\frac{d\Psi(t)}{dt}\middle|\Psi(t)\right\rangle\right)-\langle\Psi(t)|\hat{H}|\Psi(t)\rangle \tag{83}$$

and obtain equations for wave-function parameters using Euler equations, corresponding to the extremum of the Lagrangian. Using the above definition of the wave function, we find the Lagrangian in the following form:

$$\begin{aligned}\mathcal{L}=&\frac{i}{2}\sum_n(\varphi^*_n\dot{\varphi}_n-\varphi_n\dot{\varphi}^*_n)\\&+\frac{i}{2}\sum_n\varphi^*_n\varphi_n\sum_i(\dot{\alpha}_i\alpha^*_i-\dot{\alpha}^*_i\alpha_i)\\&-\sum_{nm}\varphi^*_m\varphi_n\left(\mathcal{J}_{mn}(\boldsymbol{\alpha})-\delta_{mn}\xi^{(d)}_n(\boldsymbol{\alpha})\right)\\&-\sum_n\varphi^*_n\varphi_n\sum_i\omega_i\left(\alpha^*_i\alpha_i+\frac{1}{2}\right),\end{aligned} \tag{84}$$

where we have off-diagonal modulation of couplings

$$\begin{aligned}\mathcal{J}_{mn}(\boldsymbol{\alpha})=&J_{mn}e^{-\frac{1}{2}|\boldsymbol{g}_m-\boldsymbol{g}_n|^2+(\boldsymbol{g}_m-\boldsymbol{g}_n)\cdot(\boldsymbol{\alpha}-\boldsymbol{\alpha}^*)}\\&-\delta_{mn}\sum_i\frac{2-w_i}{w_i}\omega_i g^2_{ni}\end{aligned} \tag{85}$$

and diagonal modulations (and we use g parameters instead of c):

$$\xi_n^{(d)}(\boldsymbol{\alpha}) = \sum_i \frac{1-w_i}{w_i}\omega_i g_{ni}(\alpha_i + \alpha_i^*). \tag{86}$$

Using this Lagrangian, we can write the Euler equations of motion for all parameters:

$$\frac{\partial \mathcal{L}}{\partial \varphi_i^*} - \frac{d}{dt}\frac{\partial \mathcal{L}}{\partial \dot{\varphi}_i^*} = 0, \tag{87}$$

$$\frac{\partial \mathcal{L}}{\partial \alpha_i^*} - \frac{d}{dt}\frac{\partial \mathcal{L}}{\partial \dot{\alpha}_i^*} = 0. \tag{88}$$

They yield the following equations of motion:

$$i\dot{\varphi}_n - \sum_m \left(\mathcal{J}_{nm}(\boldsymbol{\alpha}) - \delta_{mn}\xi_n^{(d)}(\boldsymbol{\alpha})\right)\varphi_m = \frac{1}{2}\varphi_n \sum_{kl} \varphi_k^*\varphi_l\left((\boldsymbol{g}_l - \boldsymbol{g}_k)\cdot(\boldsymbol{\alpha} - \boldsymbol{\alpha}^*)\mathcal{J}_{kl} - \delta_{kl}\xi_k^{(d)}\right), \tag{89}$$

$$i\dot{\alpha}_i - \omega_i\alpha_i = \sum_{mn} \varphi_m^*\varphi_n(g_{mi} - g_{ni})\mathcal{J}_{mn}(\boldsymbol{\alpha}) + \sum_n \varphi_n^*\varphi_n g_{ni}\omega_i\frac{w_i - 1}{w_i}. \tag{90}$$

We find stochastic fluctuations of the electronic amplitudes in the first equation via fluctuating $\mathcal{J}_{kl}$ and ξ_k and backaction on the phonons via the right-hand terms in the second equation. We also have a smooth transition between full polaronic description when $w = 1$ and diagonal fluctuations completely disappear to the exciton description when off-diagonal fluctuations disappear for $w = 0$.

B. Optical absorption using the variational approach for polarons

The TDVP principle describes polaron wave-function time dynamics in the electronic excited state. The optical absorption is obtained as the Fourier transform of the polarization operator expectation value, as described before. However, transforming the Hamiltonian requires transformation of all relevant operators in order to calculate expectation values, i.e., the polarization as well. We thus find the transformed polarization operator:

$$\hat{P}^{(p)} = \sum_n^{n\in\text{excited}} \boldsymbol{\mu}_{gn}(\hat{\pi}_{gn}\phi_{gn}(\hat{a}) + \hat{\pi}_{ng}\phi_{ng}(\hat{a})). \tag{91}$$

Notice that now we explicitly denote the electronic ground state and we have

$$\phi_{gn}(\hat{a}) = \exp\left(\sum_i g_{ni}\left(\hat{a}_i^\dagger - \hat{a}_i\right)\right) \tag{92}$$

and $\phi_{ng}(\hat{a}) = \phi_{gn}^\dagger(\hat{a})$. Note that the electronic ground state is described by Hamiltonian of independent oscillators:

$$\hat{H}_g = 0|g\rangle\langle g| + H_B. \tag{93}$$

The TDVP approach allows to calculate that expectation value explicitly from the wave function. So, the orientationally averaged absorption spectrum is given by the response function theory [82]:

$$\kappa(\omega) = \sum_{nn'}^{n,n'\in\text{exc}} \frac{\boldsymbol{\mu}_{gn'}\cdot\boldsymbol{\mu}_{ng}}{3}\int_0^\infty dt\; e^{i\omega t}\langle\Psi_g(t)\phi_{gn'}(\hat{a})|g\rangle \times \langle n'|\hat{G}^{(\text{pol})}(t)|n\rangle\langle g|\phi_{ng}(\hat{a})\Psi_g(0)\rangle. \tag{94}$$

Here $|\Psi_g(t)\rangle$ is the wave function in the electronic ground state, $\hat{G}^{(\text{pol})}(t)$ is the polaronic wave-function propagator in the excited state. Starting with initial ground state $|\Psi_g(0)\rangle = |g\boldsymbol{\alpha}_0\rangle$ from the right, it is projected by the transformed polarization operator onto the excited state forming the initial excited state $|\Psi_n(0)\rangle = |n\phi_{ng}(\hat{a})\boldsymbol{\alpha}_0\rangle$; $|\boldsymbol{\alpha}_0\rangle$ denotes states of all oscillators. Evolution of this state then progresses according to TDVP equations. On the left side of the expression, the initial ground state is propagated, so all bath oscillators evolve independently. Then, at time t we have $|\Psi_g(t)\rangle = |g\prod_j \exp(-i\omega_j t)\alpha_{j0}\rangle$. This state is then projected to the excited state by the transformed polarization operator.

The explicit calculation requires expressing $\phi_{ng}(\hat{a})|\boldsymbol{\alpha}_0\rangle$ due to the polaron transform. Note that we can again use the shift operator since $\phi_{gn}(\hat{a})$ also has the form of the shift operator. Then

$$\phi_{ng}(\hat{a})|\boldsymbol{\alpha}_0\rangle = \Pi_j e^{-ig_{nj}\text{Im}(\alpha_{j0})}|\alpha_{j0} - g_{nj}\rangle. \tag{95}$$

This can be included into the final expression for the absorption:

$$\kappa(\omega) = \sum_{nn'}^{n,n'\in\text{exc}} \frac{\boldsymbol{\mu}_{gn'}\cdot\boldsymbol{\mu}_{ng}}{3}\int_0^\infty dt \times e^{i\omega t}\prod_j\langle e^{-i\omega_j t}\alpha_{j0} - g_{n'j}|\alpha_j(t)\rangle \times G_{n'n}^{(\text{pol})}(t)\exp\left(-\sum_j \frac{1}{2}(g_{nj}(\alpha_{j0}^* - \alpha_{j0}) - g_{n'j}(\alpha_{j0}^* e^{i\omega_j t} - \alpha_{j0}e^{-i\omega_j t}))\right). \tag{96}$$

Here $G_{n'n}^{(\text{pol})}(t)$ is the polaronic propagator starting evolution from state $|n\Pi_j(\alpha_{j0} - g_{nj})\rangle$ and finishing at state $|n'\Pi_j\alpha_j(t)\rangle$.

V. RESULTS AND DISCUSSION

Below, we present numerical simulation results for the theories presented above. As a sample system, the same dimer is used as already presented in Sec. III A. Hence, $J_{11} = \varepsilon$, $J_{22} = \varepsilon + 200\,\text{cm}^{-1}$, while $J_{12} = J_{21} = -100$. However, in the present case the molecules are coupled to two independent sets of phonon baths, each coupled specifically to one of the two molecules. The spectral density of the two sets is identical and we use two models: the standard Drude spectral density [50],

$$C_D''(\omega) = 2\lambda\frac{\omega\gamma}{\omega^2 + \gamma^2}, \tag{97}$$

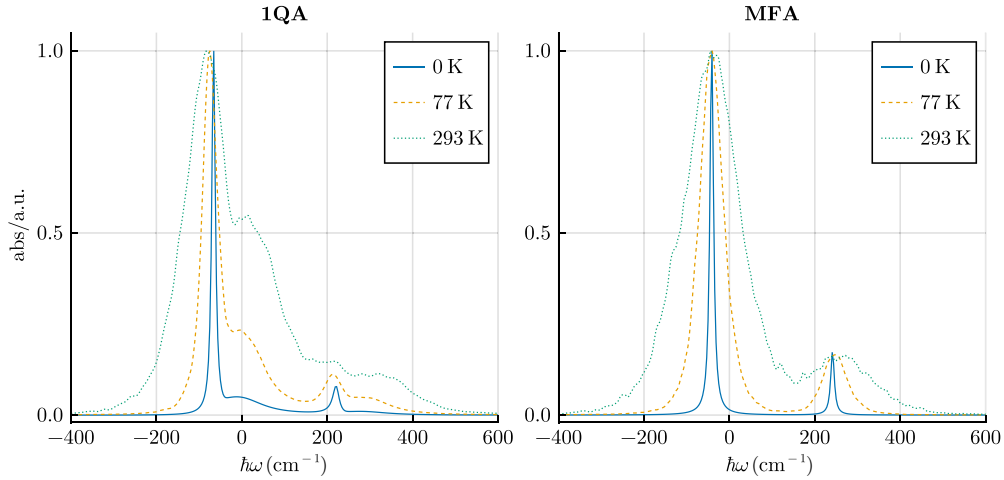


FIG. 2. The dimer absorption spectrum at different temperatures using MFA and 1QA for drude spectral density. Ensemble of 5000 trajectories was calculated for thermal averaging.

and the third degree super-Ohmic spectral density [50]:

$$C''_O(\omega) = \frac{9\lambda\pi}{2}\left(\frac{\omega}{\gamma}\right)^3 \exp\left(-\frac{3|\omega|}{\gamma}\right). \tag{98}$$

Using this form γ is the bath relaxation rate, where both types of spectral density have the maximum value, while λ is the reorganization energy. Notice that the Drude type of spectral density poorly describes absorption bands of molecules [50,59], however, it reflects the damping and decoherence process; the super-Ohmic function has correct spectral line-shape behavior around pure electronic or zero-phonon line (ZPL), however, it decays too fast at high frequencies thus restricting relaxation at large bandgaps.

For the present calculations, the bath is modeled by a set of oscillators, which span frequencies from 0 to Ω with a constant step Δ_ω. Having N bath oscillators, the coupling strengths satisfy

$$|c_j| \propto \sqrt{C''(\omega_j)}, \tag{99}$$

while they are renormalized so the total reorganization energy of oscillators matches the given value:

$$\sum_j \frac{c_j^2}{\omega_j} = \lambda. \tag{100}$$

To characterize the spectral density, we take parameters typical to pigment-protein complexes: $\gamma = \lambda = 50\,\mathrm{cm}^{-1}$. This implies approximately 100 fs decay of fluctuation correlation functions. The bath is discretized using a constant step, so $\omega_j = \Delta_\omega j$ with $\Delta_j = 1\,\mathrm{cm}^{-1}$. A single bath has $N = 500$ oscillators; for the dimer, the whole phonon manifold thus consists of 1000 oscillators (zero frequency modes are not included).

The modeling has been performed for various temperatures. The temperature is included using the statistical initialization of the phonon variables. Note that in the electronic ground state, the phonons are independent and at a given temperature the average phonon number is given by Bose-Einstein distribution $\langle \hat{a}_i^\dagger \hat{a}_i \rangle_T = (\exp(\beta\omega_i) - 1)^{-1}$. Accordingly, the harmonic oscillator fluctuations obey Gaussian statistics. As a result, the probability density of coherent states is a Gaussian:

$$P(|\alpha_i|) \propto \exp(-|\alpha_i|^2(\exp(\beta\omega_i) - 1)). \tag{101}$$

Considering the electronic ground state, these ideas can be directly applied to model specific temperature because the phonons in the electronic ground state are independent. This allows us to define α_i values in the variational model as well as a_i variables in the Heisenberg picture: the initial values for phonon variables can be taken as random Gaussian numbers with a random phase.

Consider the exciton eigenstates, which have been defined above. For the pure exciton model without the bath, the exciton energies are at -41.4 and $241.4\,\mathrm{cm}^{-1}$. As the first step, we use Drude spectral density. The exciton eigenstates are observed in absorption spectrum in the MFA calculations at zero temperature as sharp peaks, which is presented in Fig. 2 (left). The higher temperature calculations show symmetric spectral line broadening. Indeed, the phonon variables in MFA enters the equation at zero order in Eq. (47) as a classical noise. As a result, the thermal fluctuations lead to spectral broadening. At room temperature, this result is consistent, however, at zero temperature all phonon variables are at zero, hence, the broadening is vanishing.

Absorption spectra of the system at various temperatures using the 1QA is presented in Fig. 2 (right). The most obvious difference from MFA is at zero temperature, where the absorption spectrum shows emergence of asymmetric phonon side bands, consistent with quantum phenomena [49]. The sideband is obvious for the lower-energy exciton transition. In the 1QA model, the phonon side band does not involve transitions to two- or higher phonon states which should increase the side band intensity close to the excitonic peaks.

Phonon HR factors, S_{ni}, determine how many phonons are involved in electronic transition, i.e., whether the $0 \to n$ transition, where n is the number of created phonons, is observable. When $S_{ni} < 1$ for specific mode, only $0 \to 1$ phonon transition may be observed in the phonon side-band. $S_{ni} = 1$ denotes the case when $0 \to 0$ and $0 \to 1$ transitions have the same intensity, while $S_{ni} > 1$ enhances even

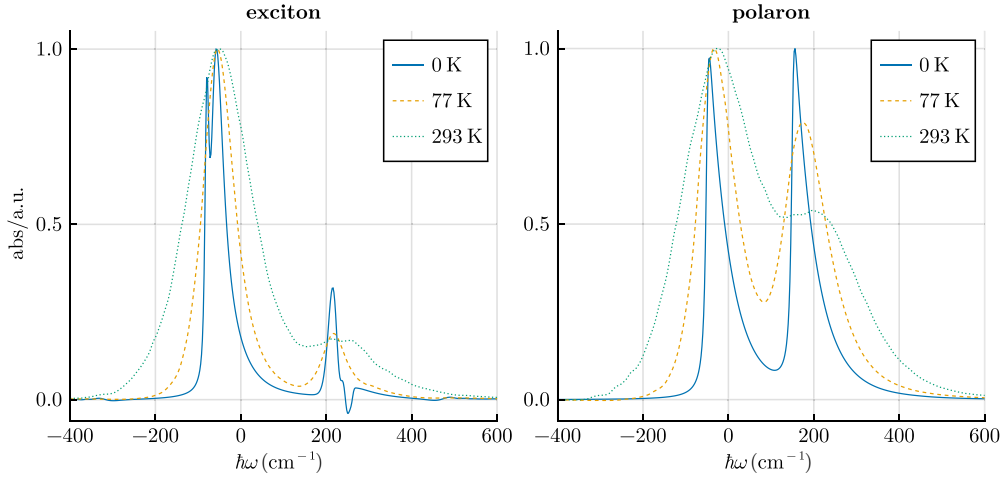


FIG. 3. The dimer absorption spectrum for drude spectral density at different temperatures using variational method for exciton and polaron models. Ensemble of 5000 trajectories was calculated for thermal averaging.

higher transitions. The amplitude of the $0 \rightarrow 1$ phonon transition (one-quantum level) is proportional to the corresponding phonon HR factor $S_{ni} = c_{ni}^2/\omega_i^2$. As $c_{ni}^2 \sim C''(\omega_i)$ for Drude model the low frequency HR factors diverge, thus, the phonon side band should approach the ZPL position as $(\omega - \omega_{\mathrm{ZPL}})^{-1}$. This is certainly not captured by 1QA. As a result, the region of very low phonon frequencies is incorrectly represented. However, for higher frequencies when $\omega_i \gg k_B T$ and when the corresponding HR factors are small, $S_i \ll 1$, the 1QA model gives correct spectral behavior at low temperature.

At higher temperatures, spectral broadening occurs due to thermally induced initial phonon occupations, so a_i variables are finite. Even in these conditions, ± 1 quantum processes are correctly represented by 1QA, so the spectral broadening in asymmetric. However, still low-frequency phonons are under-represented leading to a dip in absorption on the right shoulder of electronic peak in high temperature absorption.

The same model absorption calculation was performed using the TDVP approach and is shown in Fig. 3. The exciton model corresponds to setting all w_i values to zero. As a result, we get absorption of the excitonic TDVP model. The model is known for incorrect spectral features induced by intermolecular interactions [56]. While the lower-energy exciton peak looks correct (the split of the phonon sideband from ZPL is due to numerical finite discretization), the phonon sideband is negative for the higher exciton peak (at low temperature). Higher temperatures hide these features by broadening the spectrum similar to MFA. At room temperature, the excitonic TDVP spectrum becomes very similar to MFA calculations. Inconsistencies at low temperatures become fixed by switching to polaron model with all $w_i = 1$. In this case, phonon sidebands behave as expected for all temperatures. However, the overall intensities of the lower and higher energy exciton peaks become highly temperature dependent: At low temperature, both exciton peaks have the same intensity. This is the result that intermolecular coupling is essentially rescaled and for the Drude model becomes vanishing because of diverging HR parameters. At higher temperatures, this problem is alleviated by phonon variable randomization. At room temperature, peak line shapes as well as peak amplitudes become reasonable.

Next we switch to a more realistic super-Ohmic spectral density. The main difference from Drude spectral density is the cubic rise at low frequencies, $C''(\omega) \sim \omega^3$. As a result, the HR parameters do not diverge: $S_{ni} \sim \omega$. Such behavior should lead to characteristic ZPL and a well-distinguished phonon side band for all exciton peaks at low temperature. Such character of the peaks is completely missed in MFA simulations, as shown in Fig. 4. 1QA does capture the effect, however, the phonon side bands grow stronger with temperature, which is not realistic. A considerable improvement can be observed in TDVP modeling of absorption spectrum, as shown in Fig. 5. TDVP simulations for the lower-exciton peak in both exciton and polaron description show emergence of ZPL and the phonon sideband and merging of the two bands at higher temperatures. However, erroneous phonon sideband behavior is observed using exciton model for the higher-exciton band as the sideband is negative. This problem becomes corrected using polaron description, where the structure of absorption spectrum is coherent at all temperatures for all exciton transitions.

A specific characteristics of polaronic TDVP calculations (see Figs. 3 and 5) is that the higher intensity exciton peak has much larger relative amplitude compared to excitonic calculations. This is related to the fact that intermolecular couplings are rescaled in polaronic calculations effectively by temperature-dependent factors as demonstrated by Eq. (69). Indeed, the electronic resonant coupling is related to the transition amplitudes of the molecules (transition charge densities). The transition amplitudes are scaled by Franck-Condon factors (vibrational overlap integrals), thus, if the total reorganization energy is considerable, the intermolecular resonant coupling will be considerably reduced, which is captured by the polaron model. TDVP approach (especially polaronic model) describes optical absorption more accurately. This is specifically manifested at low temperatures, where phonon side bands are accurately reproduced. At high temperatures, all approaches reflect a proper spectral broadening. In the following, we thus focus on TDVP and

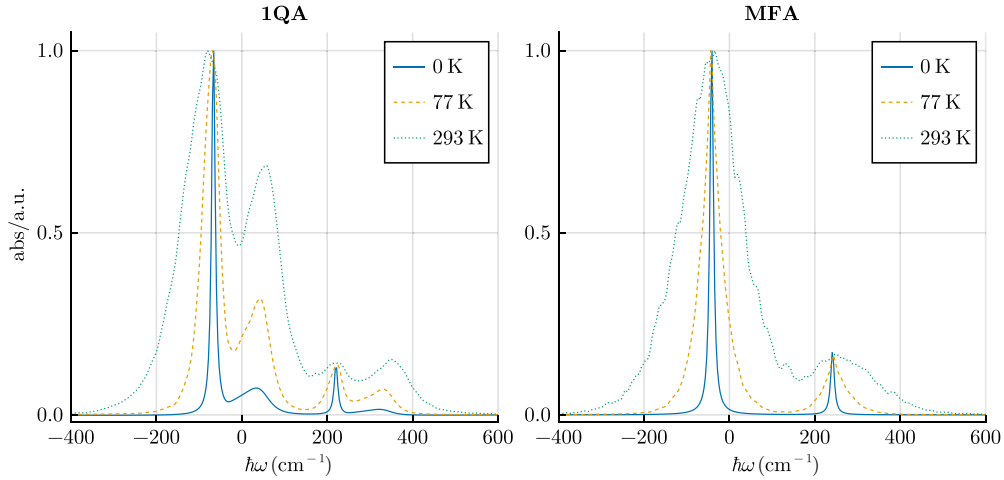


FIG. 4. The dimer absorption spectrum at different temperatures using MFA and 1QA for superohmic spectral density. Ensemble of 5000 trajectories was calculated for thermal averaging.

present excitation evolution in the excited state (after optical excitation) for two types of the bath: Drude and super-Ohmic.

As the system electronic state switches to the excited state, phonons experience a shift of global equilibrium and the phonons respond. The excitons follow and due to exciton-phonon coupling, we observe collective evolution which leads to relaxation to new equilibrium.

For the Drude spectral density, time evolution of the electronic density matrix elements, given by $\rho_{mn} = \langle \varphi_m(t)\varphi_n^*(t)\rangle$, is presented in Fig. 6. The results are presented again for both cases: exciton model $w_i = 0$ and polaron model $w_i = 1$. The zero-temperature case is not realistic, while it is presented for reference. In this case, the exciton model shows fast 300 fs relaxation of exciton coherence and of population into the new stationary state, which experiences more localization, as can be inspected from decay of exciton coherence. Hence, the self-trapped state is formed. The model shows weak prolonged oscillations, which decay within 3 ps. At 77 K temperature, the exciton model shows relaxation to the same state, while coherent oscillations decay within 500 fs. However, the self-trapping time is roughly the same as for zero temperature case. It is important to note that the self-trapping time is the same even at 293 K, which reveals itself as a fast oscillatory reorganization of exciton density matrix in first 300 fs. Later, we observe growth of population and simultaneous decay of exciton coherence. Different from lower temperatures, this signifies incoherent thermal exciton activation so higher energy states become thermally populated. Excitonic coherence however decays.

Next we switch to polaronic TDVP dynamics. However, a simplistic application of the polaronic TDVP equations runs into numerical problems due to low frequencies. This is related to the low-frequency behavior of the Drude spectral density. The coupling constants in the discretized form follow the spectral density as $c_{mi}^2 = \Delta_\omega C_n''(\omega_i)/\pi$. Additionally, oscillators at the low-frequency edge experience the high-temperature case ($\beta\omega_i < 1$), and their initial shifts grow hyperbolically as $|\alpha_i| = k_B T/\omega_i$. Then the off-diagonal fluctuating force enters the equations as $\exp(w_i(c_{mi} - c_{ni})(\alpha_i^* - \alpha_i)/\omega_i)$. For the Drude spectral density, this exponential gives extremely large amplitudes for low-frequency oscillators and equations become unstable. To overcome this

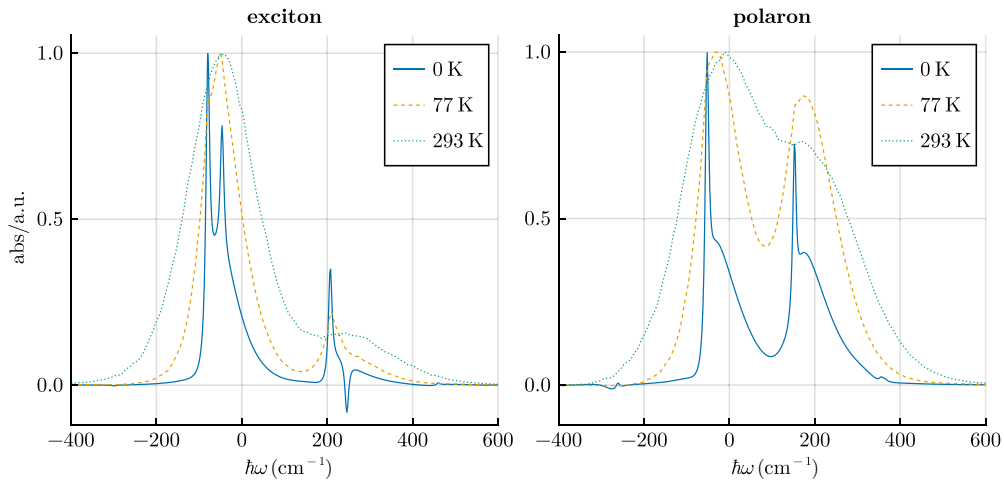


FIG. 5. The dimer absorption spectrum for superohmic spectral density at different temperatures using variational method for exciton and polaron models. Ensemble of 5000 trajectories was calculated for thermal averaging.

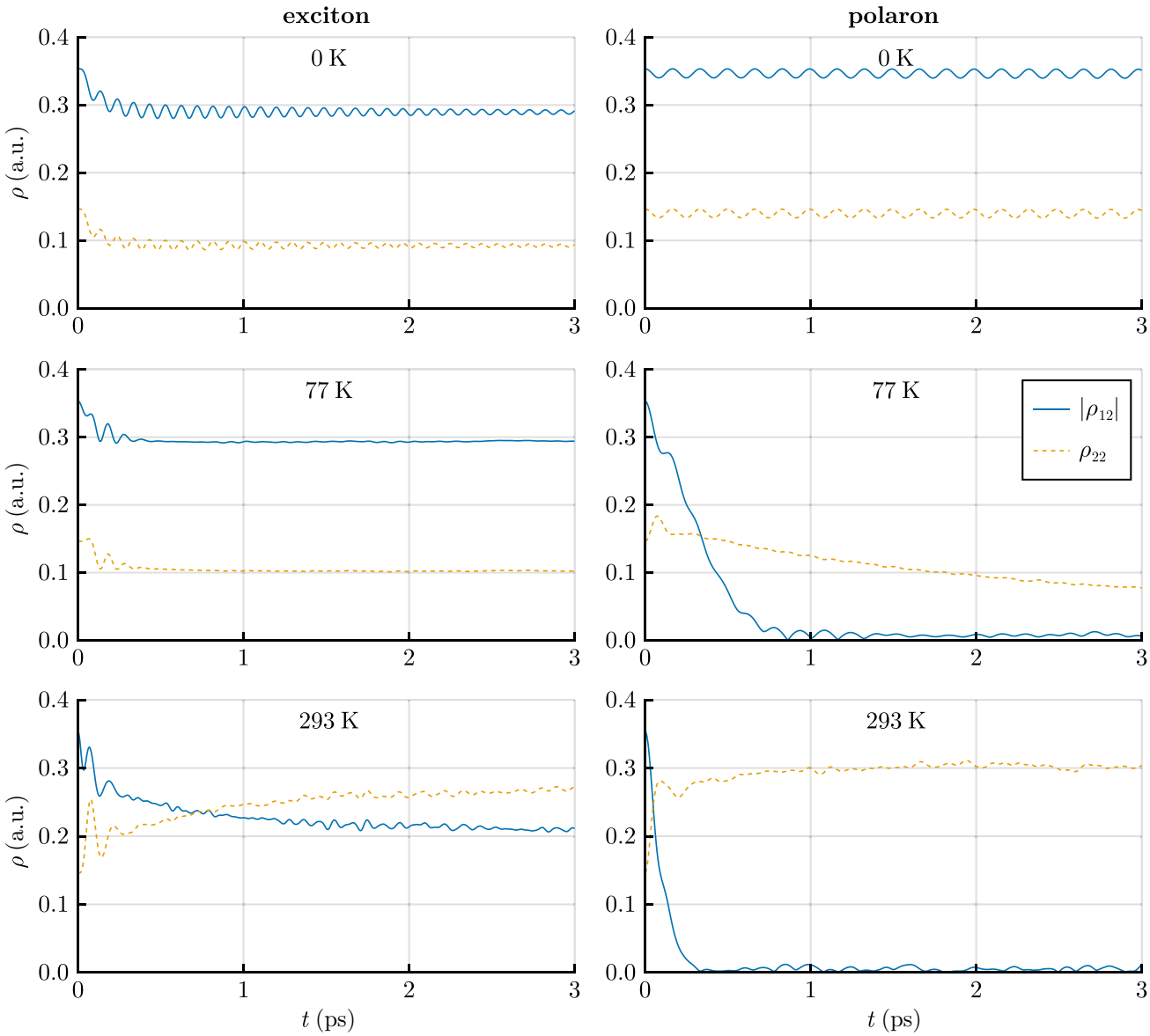


FIG. 6. Exciton density matrix dynamics starting from the lowest energy exciton state at different temperatures (top to bottom: 0 K, 77 K, 300 K) for drude spectral density. The density matrix is defined as $\rho_{mn}(t) = \langle \varphi_m(t)\varphi_n^*(t)\rangle$, where angular brackets represent the ensemble average. Orange: exciton coherence $|\rho_{12}(t)|$; black: population $\rho_{22}(t) = 1 - \rho_{11}(t)$. Left column: exciton model; right column: polaron model.

restriction for polaron modeling, the model control parameters w_i were reduced for lowest frequencies ($\omega_i < 10\,\mathrm{cm}^{-1}$) to stabilize equations. This adjustment did not affect the simulated result.

Calculated polaron dynamics are presented in Fig. 6 on the right. At zero temperature for the polaron model, the system roughly remains in the initial state and practically no evolution takes place. This may be surprising, however, that is the consequence of the Drude spectral density and zero temperature. Note that at zero temperature the effective intermolecular coupling is $\tilde{J}_{12} = J_{12}\exp(-(S_1 + S_2)/2)$, where $S_n = \sum_j S_{nj}$ are the total molecular HR factors. For the Drude spectral density $S_n \to \infty$. Thus, we find $\tilde{J}_{12} = 0$, the fluctuations at zero time vanish. As a result, the initial states become almost stationary of the variational equations. A different situation occurs at higher temperature. At 77 K, an extensive reorganization takes place during 500 fs. At this time, the system states become extensively mixed while coherences drop to < 0.1. Population redistribution takes place on longer timescale. A similar dynamics is observed at 293 K, just the damping is much faster than at 77 K, and the final population is much higher due to thermal activation.

Next we present the exciton and polaron density matrix evolution for super-Ohmic spectral density in Fig. 7. Surprisingly, the excitonic model time evolution is very similar to the Drude spectral density model. At all temperatures, there is a fast equilibration and later weak drift toward the stationary state. As the super-Ohmic spectral density has damped exciton-phonon couplings at low frequencies, the density matrix time evolution shows slight recovery after initial drop. Such evolution is not observed for Drude spectral density. An important property is the slower decay of coherences com-

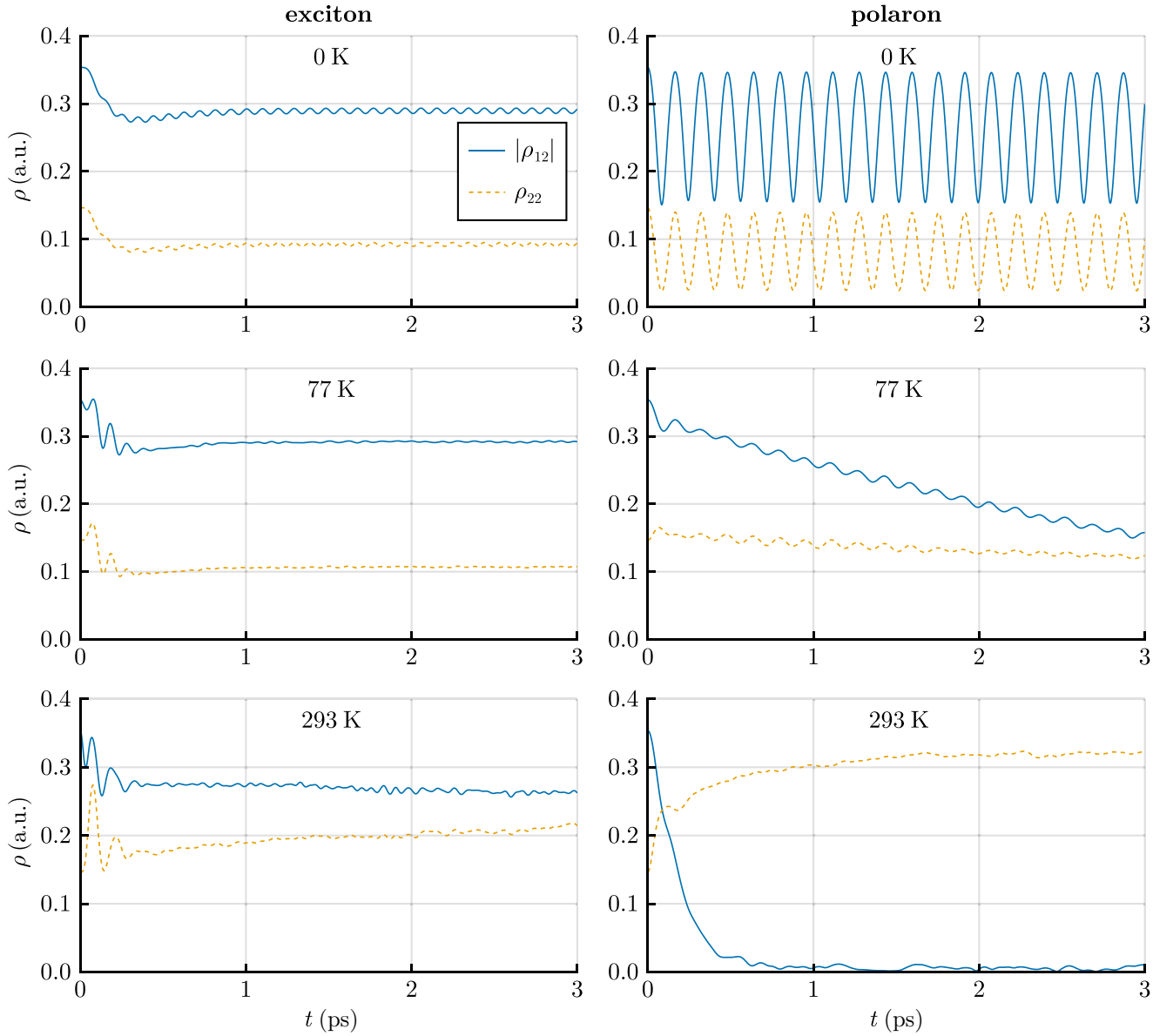


FIG. 7. Exciton density matrix dynamics starting from the lowest energy exciton state at different temperatures (top to bottom: 0 K, 77 K, 300 K) for superohmic spectral density. The density matrix is defined as $\rho_{mn}(t) = \langle \varphi_m(t)\varphi_n^*(t)\rangle$, where angular brackets represent the ensemble average. Orange: exciton coherence $|\rho_{12}(t)|$; black: population $\rho_{22}(t) = 1 - \rho_{11}(t)$. Left column: exciton model; right column: polaron model.

pared to the Drude spectral density. The super-Ohmic spectral density thus is more coherent with the same parameters, while still leading to similar relaxation patterns.

A well-recognized Redfield relaxation theory accurately describes energy and phase relaxation in the case of weak exciton-phonon interaction [13,20,67,81]. In Appendix A we have shown how the Heisenberg equations in the 1QA can be used to derive the Redfield theory using the exciton states as the reference states. Starting from the same exciton-phonon Hamiltonian and treating phonons in full quantum description (up to single phonon transitions), the Redfield theory uses several (strong) approximations, which are not implied in 1QA equations. (i) The Born approximation is used to factorize density matrix of the coupled system with the assumption that the phonons stay in thermal equilibrium at all times. (ii) The relaxation kernel is calculated to second order in the exciton-phonon coupling. (iii) Markovian approximation is performed (optional). The three approximations are satisfied in the weak exciton-phonon coupling limit. However, the approximations fail in the intermediate or strong coupling case [17]. Our 1QA equations do not involve these approximations. The phonon bath is allowed to evolve in the electronic excited state together with the excitons.

This dynamics is encapsulated in TDVP equations, which for the excitonic model are

$$i\dot{\varphi}_n - \sum_m J_{nm}\varphi_m = -\left(\xi_n^{(d)}(\boldsymbol{\alpha}) + \frac{1}{2}\sum_k \varphi_k^*\varphi_k\xi_k^{(d)}(\boldsymbol{\alpha})\right)\varphi_n, \tag{102}$$

$$i\dot{\alpha}_i - \omega_i\alpha_i = -\sum_n \varphi_n^*\varphi_n c_{ni}. \tag{103}$$

These equations are very similar to MFA [see Eqs. (33) and (34)] except from a correction in excitonic equation coming from the variational approach. These equations involve cooperative feedback relations, which allow nonequilibrium dynamics of excitons and phonons.

However, the TDVP relaxation theory is still approximate. The approximation comes from the fact that the wave function is restricted to a single Gaussian wave packet. However, the presented analysis demonstrates which of the approaches is most relevant for modeling the the exciton spectra or relaxation. Regarding the absorption spectrum at low ($\sim$0 K) temperature MFA and excitonic TDVP yield most unphysical distortions, such as incorrect phonon sidebands. 1QA and polaronic TDVP demonstrate physically sound result, which are two extremes: purely excitonic 1QA underestimates, while polaronic TDVP overestimates the higher-exciton peak and the phonon sidebands. These two descriptions can be assumed as resulting in limiting spectra, where the real spectrum lies between these two. At high (room) temperature 1QA model overestimates the phonon sideband, while other theories do not show many differences. The MFA being the simplest one can thus be used for rough estimation and again TDVP polaronic model is the opposite limiting case, where the real spectrum should be lying between them. The excitonic TDVP thus seems to be a good candidate to show various features, while their representation is poor.

Surprisingly, exciton population dynamics in the excited state is quite similar using all different theoretical models. It is important to note that coherences between excitons and polarons should not be compared because essentially the reference basis functions are different, so excitons stay coherent in the system, while polarons behave as incoherent particles in the long run. As a result, the density matrix dynamics, formulated in a polaronic picture, is sufficiently accurate for excitation dynamics, as demonstrated in Ref. [22] even with the Born approximation.

TDVP theory of polarons, which is derived in the present paper, has no Born-like approximation. Improving the theory requires adding more Gaussians per oscillator, so the wave function could become more versatile. This is the essence of the multipletic Davydov Ansatz. In this case, a single oscillator is represented by a superposition of several Gaussians. When the number of Gaussians is increased asymptotically, the theory becomes exact. It has been shown that up to five Gaussians is usually sufficient for the spectra calculation of J and H aggregates [56]. The polaronic Hamiltonian may be used for such theory as well, which is, however, beyond the scope of this paper.

Additionally, the polaron transformation requires transforming all observable operators accordingly to calculate measurable values. For absorption or exciton populations, it causes no difficulties, however, it may be complicated in general for some specific operators and may cause difficulties applying the transformation in general.

It is important to note that there is no such parameter as temperature in variational equations (unless performing optimization of transformation weight parameters as in Ref. [79]). Note that in Heisenberg equations we could fix the product to $\langle \hat{a}_i^\dagger \hat{a}_j \rangle_T = (e^{\beta\omega_j} - 1)^{-1}$ [see discussion after Eq. (A3)]. Such variable assuming the constant temperature is the well-known average phonon number. The variational equations contain simply $\alpha_j(t)$ variables, related to $\hat{a}_j$ and only their initial states are fixed. In the variational full polaron model, we can artificially construct an equation for a product $\alpha_i^*\alpha_i$, and it can be taken to have a correct asymptotic thermal equilibrium using, e.g., relaxation time approximation as done in the semiconductor Bloch equation. However, this equation does not enter the variational equations, so temperature cannot be directly incorporated.

A different approach was used in recent developments, where the equation was extended by adding stochastic scattering of the phonon amplitudes, thus leading effectively to the stochastic differential equation model [42]. In that approach, the correct temperature asymptotic limit was maintained by renormalizing phonon momenta at given scattering intervals. At the same time, this causes additional localization of exciton wave functions; hence, a high scattering rate causes fast thermalization, while strong localization. Therefore, thermalization time has to be tuned with some external information, like the experiment. In the present calculations, we included a large number of phonon modes so the thermal instability is low. However, if the number of bath oscillators is small, the oscillators may get unreasonable local heating, which needs to be addressed.

VI. CONCLUSIONS

Heisenberg equations of motion describe collective dynamics of excitons and phonons and as such allow us to capture the formation of polarons. Due to electron-phonon coupling, the stationary states involve both degrees of freedom shifted from original equilibrium values. This is denoted as exciton-polaron formation, when the exciton becomes self-trapped in polarization cloud of the environment. Such a process is properly captured within the MFA, which is essentially the semiclassical approximation. The 1QA includes quantum properties up to one phonon level. The approximation appears to be insufficient for high temperatures, when direct manifestation of multiple phonons becomes possible.

After the optical excitation, the system evolves in the excited state. The dynamics can be formulated using the TDVP scheme. The partial polaron transformation allows us to describe the excitation-polaron dynamics by choosing the most effective representation depending on the system-bath coupling as well as on the temperature.

ACKNOWLEDGMENTS

A.B. received funding from the European Union's Horizon Europe Research and Innovation Program under the Marie Skłodowska-Curie Grant Agreement No. 101119442. Computations were performed using resources at the supercomputer VU HPC Sauletekis of Vilnius University at the Faculty of Physics.

DATA AVAILABILITY

There are no publicly available research data or software supporting this manuscript. Requests for further information or data should be sent to the authors.

APPENDIX A: REDFIELD RELAXATION THEORY USING 1Q APPROXIMATION IN HEISENBERG REPRESENTATION

We start with the complete set of Heisenberg equations. At the 1QA of the theory, the one-quantum properties are explicitly maintained. We then have the set

$$-i\frac{d\pi_{kl}}{dt} = \sum_n (J_{nk}\pi_{nl} - J_{ln}\pi_{kn}) - \sum_i (c_{ki} - c_{li})(\overline{a_i\pi_{lk}}^* + \overline{a_i\pi_{kl}}), \tag{A1}$$

$$-i\frac{d\overline{a_j\pi_{kl}}}{dt} = -\omega_j\overline{a_j\pi_{kl}} + \sum_n (J_{nk}\overline{a_j\pi_{nl}} - J_{ln}\overline{a_j\pi_{kn}}) - \sum_i (c_{ki} - c_{li})\overline{a_i'a_j\pi_{kl}} + c_{lj}\pi_{kl}, \tag{A2}$$

$$-i\frac{d\overline{a_i'a_j\pi_{kl}}}{dt} = (\omega_i - \omega_j)\overline{a_i'a_j\pi_{kl}} + \sum_n (J_{nk}\overline{a_i'a_j\pi_{nl}} - J_{ln}\overline{a_i'a_j\pi_{kn}}) + c_{kj}\overline{a_i\pi_{lk}}^* - c_{ki}\overline{a_j\pi_{kl}}. \tag{A3}$$

Note that $\langle\hat{a}_j\hat{a}_i\hat{\pi}_{kl}\rangle$ is a two-quanta variable, which is neglected, while $\overline{a_i\pi_{lk}}^* = \overline{a_i'\pi_{kl}}$. The three equations thus form the closed set of equations which explicitly include properties of one-phonon excitations. This set of equations still maintains system and bath correlations at all times. If equations are used to describe nonequilibrium conditions, for example, after optical excitation, the correlation between the system and the bath at initial time can be neglected. The initial conditions can then be written as $\overline{a\pi}_{jkl}(0) = a_j(0)\pi_{kl}(0)$, $\overline{a_i'a_j\pi_{kl}}(0) = \delta_{ji}\langle\hat{a}_j^\dagger\hat{a}_j\rangle_T\pi_{kl}(0)$, here $\langle\hat{a}_j^\dagger\hat{a}_j\rangle_T = 1/(e^{i\omega_j} - 1)$ denotes the thermal average occupation number.

A separate description of the thermal initial condition for $a_j(0)$ is necessary when $\beta\omega_j$ is not vanishing. $a_j(t)$ at thermal equilibrium performs Gaussian fluctuations such that the dispersion $\langle|a_j(t)|^2\rangle = \langle\hat{a}_j^\dagger\hat{a}_j\rangle_T$. Therefore, we can write the Gaussian probability density

$$p(|a_j|) = \nu_j \exp(-|a_j|^2(e^{i\omega_j} - 1)), \tag{A4}$$

ν_α being a normalization factor, which leads to correct thermal average and is denoted as the Glauber–Sudarshan P representation. At thermal equilibrium for an isolated oscillator $|a_j|$ is thus given by a Gaussian random number, while the phase is not defined, hence $a_j = |a_j|\exp(i\eta)$, where $0 < \eta < 2\pi$ is a random phase.

These equations can be used to derive the Redfield relaxation equations, which hold for the weak system-bath coupling, i.e., when only single-quantum excitations are important. Additionally, in the Redfield theory, the bath is always at equilibrium and does not respond to the system state. In this case, the correlation between different oscillators is absent and the system-bath interaction can be neglected in the third equation, which yields thermal average $\overline{a_i'a_j\pi_{kl}}(t) = \delta_{ji}\langle\hat{a}_j^\dagger\hat{a}_j\rangle_T\pi_{kl}(t)$ at all times. From the second equation, we can rewrite the equation in the following form:

$$-i\frac{d\overline{a_j\pi_{kl}}}{dt} = -\omega_j\overline{a_j\pi_{kl}} + \sum_n (J_{nk}\overline{a_j\pi_{nl}} - J_{ln}\overline{a_j\pi_{kn}}) - \sum_i (c_{ki} - c_{li})\overline{a_i'a_j\pi_{kl}} + c_{lj}\pi_{kl}, \tag{A5}$$

and there is still no average, only variables. Using $\hat{a}_i^\dagger\hat{a}_j + \delta_{ji} = \hat{a}_j\hat{a}_i^\dagger$, then we solve the equation

$$\overline{a_j\pi_{kl}}(t) = i\int_{-\infty}^{t} d\tau e^{-i\omega_j(t-\tau)}e_{km}^{iJ(t-\tau)} \times \sum_i (c_{ni}\overline{a_j a_i'\pi_{mn}}(\tau) - c_{mi}\overline{a_i'a_j\pi_{mn}}(\tau))e_{nl}^{-iJ(t-\tau)}. \tag{A6}$$

Here, on the right-hand side, we imply summation over m and n, e_{kl}^{iJt} is the matrix exponential. Then, similarly,

$$\overline{a_j'\pi_{kl}}(t) = i\int_{-\infty}^{t} d\tau e^{i\omega_j(t-\tau)}e_{km}^{iJ(t-\tau)} \times \sum_i (c_{ni}\overline{a_j' a_i\pi_{mn}}(\tau) - c_{mi}\overline{a_i a_j'\pi_{mn}}(\tau))e_{nl}^{-iJ(t-\tau)}. \tag{A7}$$

Next, we substitute this result into the first equation, make thermal average, and using the coordinate-correlation function

$$\langle\hat{a}^\dagger{}_i(t)\hat{a}_i(\tau)\rangle + \langle\hat{a}_i(t)\hat{a}_i^\dagger(\tau)\rangle = \frac{1}{2}C_i(t-\tau), \tag{A8}$$

one gets an equation which directly corresponds to the convolutional Redfield relaxation equation [13,20,68,81]:

$$\frac{d\pi_{kl}}{dt} = i\sum_n (J_{nk}\pi_{nl} - J_{ln}\pi_{kn}) - \int_0^\infty d\tau \sum_{mn} \mathcal{R}_{kl,mn}(\tau)\pi_{mn}(t-\tau), \tag{A9}$$

where

$$\mathcal{R}_{kl,mn}(\tau) = \sum_i (c_{li} - c_{ki})e_{km}^{iJ\tau}e_{nl}^{-iJ\tau} \times (c_{ni}C_i(\tau) - c_{mi}C_i^*(\tau)). \tag{A10}$$

The expression is obtained by additionally using the requirement for thermal average at all times.

APPENDIX B: MAIN PROPERTIES OF COHERENT STATES

The time-dependent variational principle approach is formulated using the coherent state basis, which is very effective for quantum harmonic oscillators. Coherent states are basic ingredients characterizing highly excited semiclassical pure states, which are the main ingredients in optical radiation theory for photons and in vibrational theory for phonons. Both systems are essentially described by the same type of harmonic oscillators.

A quantum harmonic oscillator Hamiltonian is given by

$$\hat{H} = \hbar\omega\left(\hat{a}^\dagger\hat{a} + \tfrac{1}{2}\right). \tag{B1}$$

Here ω is the oscillator frequency, $\hat{a}^\dagger$ is the quantum creation operator, while $\hat{a}$ the corresponding annihilation operator. The so-called Fock or number states of the oscillator are generated from the ground-vacuum state $|0\rangle$ starting from $n = 1$:

$$|n\rangle = \sqrt{n}\hat{a}^\dagger|0\rangle. \tag{B2}$$

The opposite direction:

$$|n-1\rangle = \sqrt{n}\hat{a}|n\rangle. \tag{B3}$$

The product $\hat{a}^\dagger\hat{a}|n\rangle = n|n\rangle$ is the number operator, while state $|n\rangle$ is the eigenstate of the Hamiltonian. The creation and annihilation operator satisfies the commutation relation:

$$[\hat{a}, \hat{a}^\dagger] = 1. \tag{B4}$$

The number state is hence the eigenstate of the number operator.

Another set of states is generated by the eigenequation for the annihilation operator:

$$\hat{a}|\alpha\rangle = \alpha|\alpha\rangle. \tag{B5}$$

Here $|\alpha\rangle$ is the coherent state, while α is the corresponding eigenvalue.

To find the expression for $|\alpha\rangle$ it can be expanded in the number states:

$$|\alpha\rangle = \exp\left(-\frac{|\alpha|^2}{2}\right)\sum_n \frac{\alpha^n}{\sqrt{n!}}|n\rangle. \tag{B6}$$

The coherent states are normalized, while not orthogonal:

$$\langle\alpha|\beta\rangle = \exp\left(\alpha^*\beta - \frac{|\alpha|^2}{2} - \frac{|\beta|^2}{2}\right) \tag{B7}$$

and also

$$|\langle\alpha|\beta\rangle|^2 = \exp(-|\alpha-\beta|^2). \tag{B8}$$

Additional properties of the coherent states are that the expectation value of the coordinate operator is

$$\langle\alpha|\hat{x}|\alpha\rangle = R(\alpha), \tag{B9}$$

while that of the momentum operator is

$$\langle\alpha|\hat{p}|\alpha\rangle = \mathrm{Im}(\alpha). \tag{B10}$$

Coherent states are also generated by the shift operator

$$\hat{D}(\alpha) = \exp(\alpha\hat{a}^\dagger - \alpha^*\hat{a}) \tag{B11}$$

and is known as the shift operator

$$|\alpha\rangle = \hat{D}(\alpha)|0\rangle. \tag{B12}$$

It can be shown that the coordinate and momentum variances are the same as of the ground state of the Harmonic oscillator. Thus, the coherent state is equivalent to the ground state of the Harmonic oscillator, which is a Gaussian wave packet, that is shifted by α in the phase space of the oscillator.

Next we describe some properties related to the shift operator. First, using Weyl formula

$$\exp(\hat{A})\exp(\hat{B}) = \exp(\hat{A}+\hat{B})\exp\left(\tfrac{1}{2}[\hat{A},\hat{B}]\right), \tag{B13}$$

the shift operator can be factorized:

$$\exp(\alpha\hat{a}^\dagger)\exp(-\alpha^*\hat{a})\exp\left(\frac{|\alpha|^2}{2}\right) = \exp(\alpha\hat{a}^\dagger - \alpha^*\hat{a}), \tag{B14}$$

which is useful in calculating various operator properties and is extensively used to derive all the equations in this paper. It can be easily checked that $\hat{D}(0) = I$, so $\hat{D}^n(\alpha) = \hat{D}(n\alpha)$ and $\hat{D}(-\alpha) = \hat{D}^\dagger(\alpha)$. Using the above relations, we directly find

$$D(\alpha)D(\beta) = \exp\left(\tfrac{1}{2}(\alpha\beta^* - \alpha^*\beta)\right)D(\alpha+\beta). \tag{B15}$$

[1] A. S. Davydov, *Theory of Molecular Excitons* (Springer, New York, NY, 1971).

[2] M. Pope and C. E. Swenberg, *Electronic Processes in Organic Crystals and Polymers*, 2nd ed. (Oxford Academic, New York, NY, 1999).

[3] H. van Amerongen, L. Valkunas, and R. van Grondelle, *Photosynthetic Excitons* (World Scientific, Singapore, 2006).

[4] R. E. Blankenship, *Molecular Mechanisms of Photosynthesis*, 2nd ed. (Wiley Blackwell, Chichester, West Sussex, UK, 2014).

[5] V. Sláma, L. Cupellini, and B. Mennucci, Excitonic nature of carotenoid–phthalocyanine dyads and its role in transient absorption spectra, ACS Phys. Chem Au **2**, 206 (2022).

[6] I. G. Prandi, L. Viani, O. Andreussi, and B. Mennucci, Combining classical molecular dynamics and quantum mechanical methods for the description of electronic excitations: The case of carotenoids, J. Comput. Chem. **37**, 981 (2016).

[7] E. Romero, V. I. Novoderezhkin, and R. van Grondelle, Quantum design of photosynthesis for bio-inspired solar-energy conversion, Nature (London) **543**, 355 (2017).

[8] V. L. Broude, E. I. Rashba, and E. F. Sheka, *Spectroscopy of Molecular Excitons* (Springer-Verlag, New York, NY, 1985).

[9] Edited by E. I. Rashba and M. D. Sturge, *Excitons, Vol. 2, Modern Problems in Condensed Matter Sciences* (North-Holland, Amsterdam/New York, 1982).

[10] L. Landau, The movement of electrons in the crystal lattice, Phys. Z. Sowjetunion **3**, 644 (1933).

[11] M. Grover and R. Silbey, Exciton migration in molecular crystals, J. Chem. Phys. **54**, 4843 (1971).

[12] A. G. Redfield, On the theory of relaxation processes, IBM J. Res. Dev. **1**, 19 (1957).

[13] H. P. Breuer and F. Petruccione, *The Theory of Open Quantum Systems* (Oxford University Press, Oxford, 2007).

[14] A. Ishizaki, T. R. Calhoun, G. S. Schlau-Cohen, and G. R. Fleming, Quantum coherence and its interplay with protein environments in photosynthetic electronic energy transfer, Phys. Chem. Chem. Phys. **12**, 7319 (2010).

[15] S. Korsakas, J. Bučinskas, and D. Abramavicius, Long memory effects in excitonic systems dynamics: Spectral relations and excitation transport, J. Chem. Phys. **152**, 244114 (2020).

[16] W. M. Zhang, T. Meier, V. Chernyak, and S. Mukamel, Exciton-migration and three-pulse femtosecond optical spectroscopies of photosynthetic antenna complexes, J. Chem. Phys. **108**, 7763 (1998).

[17] A. Ishizaki and G. R. Fleming, On the adequacy of the Redfield equation and related approaches to the study of quantum dynamics in electronic energy transfer, J. Chem. Phys. **130**, 234110 (2009).
[18] A. Fruchtman, N. Lambert, and E. M. Gauger, When do perturbative approaches accurately capture the dynamics of complex quantum systems? Sci. Rep. **6**, 28204 (2016).
[19] D. Abramavicius, B. Palmieri, D. V. Voronine, F. Šanda, and S. Mukamel, Coherent multidimensional optical spectroscopy of excitons in molecular aggregates; quasiparticle versus supermolecule perspectives, Chem. Rev. **109**, 2350 (2009).
[20] V. May and O. Kühn, *Charge and Energy Transfer Dynamics in Molecular Systems*, 3rd ed. (Wiley-VCH, Weinheim, 2011).
[21] S. Jang, J. Cao, and R. J. Silbey, Fourth-order quantum master equation and its Markovian bath limit, J. Chem. Phys. **116**, 2705 (2002).
[22] S. J. Jang, Partially polaron-transformed quantum master equation for exciton and charge transport dynamics, J. Chem. Phys. **157**, 104107 (2022).
[23] U. Weiss, *Quantum Dissipative Systems* (World Scientific, Singapore, Hackensack, 2012).
[24] A. J. Leggett, S. Chakravarty, A. T. Dorsey, M. P. Fisher, A. Garg, and W. Zwerger, Dynamics of the dissipative two-state system, Rev. Mod. Phys. **59**, 1 (1987).
[25] Y. Tanimura, Numerically "exact" approach to open quantum dynamics: The hierarchical equations of motion (HEOM), J. Chem. Phys. **153**, 020901 (2020).
[26] Y. Tanimura, Stochastic Liouville, Langevin, Fokker–Planck, and master equation approaches to quantum dissipative systems, J. Phys. Soc. Jpn. **75**, 082001 (2006).
[27] J. J. Ding, J. Xu, J. Hu, R. X. Xu, and Y. Yan, Optimized hierarchical equations of motion theory for Drude dissipation and efficient implementation to nonlinear spectroscopies, J. Chem. Phys. **135**, 164107 (2011).
[28] J. Xu, R.-X. Xu, D. Abramavicius, H.-D. Zhang, and Y.-J. Yan, Advancing hierarchical equations of motion for efficient evaluation of coherent two-dimensional spectroscopy, Chin. J. Chem. Phys. **24**, 497 (2011).
[29] C. Curutchet and B. Mennucci, Quantum chemical studies of light harvesting, Chem. Rev. **117**, 294 (2017).
[30] A. Gelzinis, D. Abramavicius, and L. Valkunas, Absorption lineshapes of molecular aggregates revisited, J. Chem. Phys. **142**, 154107 (2015).
[31] F. D. Fuller, J. Pan, A. Gelzinis, V. Butkus, S. Senlik, D. E. Wilcox, C. F. Yocum, L. Valkunas, D. Abramavicius, and J. P. Ogilvie, Vibronic coherence in oxygenic photosynthesis, Nat. Chem. **6**, 706 (2014).
[32] J. Chmeliov, A. Gelzinis, E. Songaila, R. Augulis, C. D. Duffy, A. V. Ruban, and L. Valkunas, The nature of self-regulation in photosynthetic light-harvesting antenna, Nat. Plants **2**, 16045 (2016).
[33] D. Loco, S. Jurinovich, L. Cupellini, M. F. S. J. Menger, and B. Mennucci, The modeling of the absorption lineshape for embedded molecules through a polarizable QM/MM approach, Photochem. Photobiol. Sci. **17**, 552 (2018).
[34] E. Cignoni, V. Slama, L. Cupellini, and B. Mennucci, The atomistic modeling of light-harvesting complexes from the physical models to the computational protocol, J. Chem. Phys. **156**, 120901 (2022).
[35] P. E. Parris and V. M. Kenkre, Variational considerations in the study of carrier transport in organic crystals, Phys. Rev. B **70**, 064304 (2004).
[36] J. Sun, L. Duan, and Y. Zhao, Delocalized Davydov D_1 *Ansatz* for the Holstein polaron, J. Chem. Phys. **138**, 174116 (2013).
[37] L. Chen, M. Gelin, and Y. Zhao, Dynamics of the spin-boson model: A comparison of the multiple Davydov $D_1, D_{1.5}, D_2$ Ansätze, Chem. Phys. **515**, 108 (2018).
[38] V. Chorošajev, O. Rancova, and D. Abramavicius, Polaronic effects at finite temperatures in the B850 ring of the LH2 complex, Phys. Chem. Chem. Phys. **18**, 7966 (2016).
[39] V. Chorošajev, A. Gelzinis, L. Valkunas, and D. Abramavicius, Dynamics of exciton-polaron transition in molecular assemblies: The variational approach, J. Chem. Phys. **140**, 244108 (2014).
[40] L. Chen and Y. Zhao, Finite temperature dynamics of a Holstein polaron: The thermo-field dynamics approach, J. Chem. Phys. **147**, 214102 (2017).
[41] D. Abramavicius, V. Chorošajev, and L. Valkunas, Tracing feed-back driven exciton dynamics in molecular aggregates, Phys. Chem. Chem. Phys. **20**, 21225 (2018).
[42] M. Jakučionis and D. Abramavičius, Temperature-controlled open-quantum-system dynamics using a time-dependent variational method, Phys. Rev. A **103**, 032202 (2021).
[43] V. Balevičius Jr, T. Wei, D. Di Tommaso, D. Abramavicius, J. Hauer, T. Polívka, and C. D. P. Duffy, The full dynamics of energy relaxation in large organic molecules: From photoexcitation to solvent heating, Chem. Sci. **10**, 4792 (2019).
[44] A. Raab, I. Burghardt, and H.-D. Meyer, The multiconfiguration time-dependent Hartree method generalized to the propagation of density operators, J. Chem. Phys. **111**, 8759 (1999).
[45] M. Schröter, S. D. Ivanov, J. Schulze, S. P. Polyutov, Y. Yan, T. Pullerits, and O. Kühn, Exciton–vibrational coupling in the dynamics and spectroscopy of Frenkel excitons in molecular aggregates, Phys. Rep. **567**, 1 (2015).
[46] M. Jakučionis and D. Abramavičius, Thermalization of open quantum systems using the multiple-Davydov-D_2 variational approach, Phys. Rev. A **107**, 062205 (2023).
[47] Y. Zhao, K. Sun, L. Chen, and M. Gelin, The hierarchy of Davydov's Ansätze and its applications, WIREs Comput. Mol. Sci. **12**, e1589 (2022).
[48] A. Mikalčiūtė and D. Abramavičius, Complete exciton Hamiltonian for photosynthetic pigment–protein complexes, J. Chem. Phys. **162**, 164109 (2025).
[49] R. Jankowiak, M. Reppert, V. Zazubovich, J. Pieper, and T. Reinot, Site selective and single complex laser-based spectroscopies: A window on excited state electronic structure, excitation energy transfer, and electron–phonon coupling of selected photosynthetic complexes, Chem. Rev. **111**, 4546 (2011).
[50] A. Kell, X. Feng, M. Reppert, and R. Jankowiak, On the shape of the phonon spectral density in photosynthetic complexes, J. Phys. Chem. B **117**, 7317 (2013).
[51] A. Anda, L. D. Vico, T. Hansen, and D. Abramavičius, Absorption and fluorescence lineshape theory for polynomial potentials, J. Chem. Theory Comput. **12**, 5979 (2016).
[52] T. J. Zuehlsdorff, A. Montoya-Castillo, J. A. Napoli, T. E. Markland, and C. M. Isborn, Optical spectra in the condensed phase: Capturing anharmonic and vibronic features using dynamic and static approaches, J. Chem. Phys. **151**, 074111 (2019).

[53] L. Allan and T. J. Zuehlsdorff, Taming the third order cumulant approximation to linear optical spectroscopy, J. Chem. Phys. **160**, 074108 (2024).
[54] M. L. Chaillet, F. Lengauer, J. Adolphs, F. Müh, A. S. Fokas, D. J. Cole, A. W. Chin, and T. Renger, Static disorder in excitation energies of the Fenna–Matthews–Olson protein: Structure-based theory meets experiment, J. Phys. Chem. Lett. **11**, 10306 (2020).
[55] E. Bašinskaitė, V. Butkus, D. Abramavicius, and L. Valkunas, Vibronic models for nonlinear spectroscopy simulations, Photosynth. Res. **121**, 95 (2014).
[56] M. Jakučionis, A. Žukas, and D. Abramavičius, Modeling molecular J and H aggregates using multiple-Davydov D2 ansatz, Phys. Chem. Chem. Phys. **24**, 17665 (2022).
[57] O. Rancova, M. Jakučionis, L. Valkunas, and D. Abramavicius, Origin of non-Gaussian site energy disorder in molecular aggregates, Chem. Phys. Lett. **674**, 120 (2017).
[58] O. Rancova, R. Jankowiak, and D. Abramavicius, Role of bath fluctuations in the double-excitation manifold in shaping the 2DES of bacterial reaction centers at low temperature, J. Phys. Chem. B **122**, 1348 (2018).
[59] O. Rancova, R. Jankowiak, and D. Abramavicius, Probing environment fluctuations by two-dimensional electronic spectroscopy of molecular systems at temperatures below 5 K, J. Chem. Phys. **142**, 212428 (2015).
[60] A. C. Newell and J. V. Moloney, *Nonlinear Optics* (Westview Press, Boulder, CO, 2004).
[61] F. C. Spano and S. Mukamel, Nonlinear susceptibilities of molecular aggregates: Enhancement of $\chi^{(3)}$ by size, Phys. Rev. A **40**, 5783 (1989).
[62] J. A. Leegwater and S. Mukamel, Exciton-scattering mechanism for enhanced nonlinear response of molecular nanostructures, Phys. Rev. A **46**, 452 (1992).
[63] V. Chernyak, W. M. Zhang, and S. Mukamel, Multidimensional femtosecond spectroscopies of molecular aggregates and semiconductor nanostructures: The nonlinear exciton equations, J. Chem. Phys. **109**, 9587 (1998).
[64] S. Mukamel and D. Abramavicius, Many-body approaches for simulating coherent nonlinear spectroscopies of electronic and vibrational excitons, Chem. Rev. **104**, 2073 (2004).
[65] V. Bubilaitis and D. Abramavicius, Signatures of exciton–exciton annihilation in 2DES spectra including up to six-wave mixing processes, J. Chem. Phys. **161**, 104106 (2024).
[66] V. Bubilaitis and D. Abramavicius, Compact modeling of highly excited linear aggregates using generalized quantum particles, Chem. Phys. **588**, 112445 (2025).
[67] V. M. Axt and S. Mukamel, Nonlinear optics of semiconductor and molecular nanostructures; a common perspective, Rev. Mod. Phys. **70**, 145 (1998).
[68] F. Rossi and T. Kuhn, Theory of ultrafast phenomena in photoexcited semiconductors, Rev. Mod. Phys. **74**, 895 (2002).
[69] N. W. Ashcroft and N. D. Mermin, *Solid State Physics* (Thomson Learning Inc., New York, 1976).
[70] T. Kobayashi, *J-Aggregates* (World Scientific Publishing Company, Singapore, River Edge, NJ, 1996).
[71] S. Ramesh, Y. Wang, P. Chabera, R. Araujo, M. Aboulsaad, T. Edvinsson, F. Gao, and T. Pullerits, Coherent phonons, localization, and slow polaron formation in lead-free gold perovskite, Adv. Opt. Mater. **13**, 2402882 (2025).
[72] K. Zheng, M. Abdellah, Q. Zhu, Q. Kong, G. Jennings, C. A. Kurtz, M. E. Messing, Y. Niu, D. J. Gosztola, M. J. Al-Marri, X. Zhang, T. Pullerits, and S. E. Canton, Direct experimental evidence for photoinduced strong-coupling polarons in organolead halide perovskite nanoparticles, J. Phys. Chem. Lett. **7**, 4535 (2016).
[73] F. Thouin, D. A. Valverde-Chvez, C. Quarti, D. Cortecchia, I. Bargigia, D. Beljonne, A. Petrozza, C. Silva, and A. R. S. Kandada, Phonon coherences reveal the polaronic character of excitons in two-dimensional lead halide perovskites, Nat. Mater. **18**, 349 (2019).
[74] M. D. Smith, A. Jaffe, E. R. Dohner, A. M. Lindenberg, and H. I. Karunadasa, Structural origins of broadband emission from layered Pb–Br hybrid perovskites, Chem. Sci. **8**, 4497 (2017).
[75] M. R. Philpott, Theory of the coupling of electronic and vibrational excitations in molecular crystals and helical polymers, J. Chem. Phys. **55**, 2039 (1971).
[76] F. C. Spano, The spectral signatures of Frenkel polarons in H- and J-aggregates, Acc. Chem. Res. **43**, 429 (2010).
[77] S. Polyutov, O. Kühn, and T. Pullerits, Exciton-vibrational coupling in molecular aggregates: Electronic versus vibronic dimer, Chem. Phys. **394**, 21 (2012).
[78] A. Chenu, N. Christensson, H. F. Kauffmann, and T. Mančal, Enhancement of vibronic and ground-state vibrational coherences in 2D spectra of photosynthetic complexes, Sci. Rep. **3**, 2029 (2013).
[79] Y.-C. Cheng and R. J. Silbey, A unified theory for charge-carrier transport in organic crystals, J. Chem. Phys. **128**, 114713 (2008).
[80] D. R. Yarkony and R. Silbey, Variational approach to exciton transport in molecular crystals, J. Chem. Phys. **67**, 5818 (1977).
[81] L. Valkunas, D. Abramavicius, and T. Mančal, *Molecular Excitation Dynamics and Relaxation* (Wiley-VCH Verlag GmbH & Co. KGaA, 2013).
[82] S. Mukamel, *Principles of Nonlinear Optical Spectroscopy* (Oxford University Press, New York, 1995).